

## Accepted Manuscript

Title: Liquid chromatography-quadrupole time-of-flight mass spectrometry for screening *in vitro* drug metabolites in humans: investigation on seven phenethylamine-based designer drugs

Author: Foon Yin Lai Claudio Erratico Juliet Kinyua Jochen F. Mueller Adrian Covaci Alexander L.N.van Nuijs

PII: S0731-7085(15)30036-4  
DOI: <http://dx.doi.org/doi:10.1016/j.jpba.2015.06.016>  
Reference: PBA 10134

To appear in: *Journal of Pharmaceutical and Biomedical Analysis*

Received date: 10-3-2015  
Revised date: 4-6-2015  
Accepted date: 10-6-2015

Please cite this article as: Foon Yin Lai, Claudio Erratico, Juliet Kinyua, Jochen F.Mueller, Adrian Covaci, Alexander L.N.van Nuijs, Liquid chromatography-quadrupole time-of-flight mass spectrometry for screening *in vitro* drug metabolites in humans: investigation on seven phenethylamine-based designer drugs, *Journal of Pharmaceutical and Biomedical Analysis* <http://dx.doi.org/10.1016/j.jpba.2015.06.016>

This is a PDF file of an unedited manuscript that has been accepted for publication. As a service to our customers we are providing this early version of the manuscript. The manuscript will undergo copyediting, typesetting, and review of the resulting proof before it is published in its final form. Please note that during the production process errors may be discovered which could affect the content, and all legal disclaimers that apply to the journal pertain.



1 **Liquid chromatography-quadrupole time-of-flight mass spectrometry for screening *in***  
2 ***vitro* drug metabolites in humans: investigation on seven phenethylamine-based**  
3 **designer drugs**

4  
5 Foon Yin Lai<sup>a,\*</sup>, Claudio Erratico<sup>b</sup>, Juliet Kinyua<sup>b</sup>, Jochen F. Mueller<sup>a</sup>, Adrian Covaci<sup>b,\*</sup>,  
6 Alexander L.N. van Nuijs<sup>b</sup>

7  
8 a. The University of Queensland, The National Research Centre for Environmental  
9 Toxicology, 39 Kessels Road, Coopers Plains, QLD 4108, Australia

10 b. Toxicological Center, University of Antwerp, Universiteitsplein 1, 2610 Antwerp,  
11 Belgium

12  
13  
14 \*Corresponding authors' details:

15 Dr. Foon Yin Lai: The University of Queensland, The National Research Centre for  
16 Environmental Toxicology (Entox), 39 Kessels Road, Coopers Plains, QLD 4108, Australia.

17 Tel.: +61 (0)4 06714601; Fax.: +61 (0)7 3274 9003; E-mail: [foon.lai@uqconnect.edu.au](mailto:foon.lai@uqconnect.edu.au)

18 Prof. Dr. Adrian Covaci: Toxicological Center, Universiteit Antwerpen, Universiteitsplein 1,  
19 2610 Wilrijk-Antwerpen, Belgium.

20 Tel.: +32 3 265 24 98; E-mail: [adrian.covaci@uantwerpen.be](mailto:adrian.covaci@uantwerpen.be)

21

22

23 **Abstract**

24 Phenethylamine-based designer drugs are prevalent within the new psychoactive substance  
25 market. Characterisation of their metabolites is important in order to identify suitable  
26 biomarkers which can be used for better monitoring their consumption. Careful design of *in*  
27 *vitro* metabolism experiments using subcellular liver fractions will assist in obtaining reliable  
28 outcomes for such purposes. The objective of this study was to stepwise investigate the *in*  
29 *vitro* human metabolism of seven phenethylamine-based designer drugs using individual  
30 families of enzymes. This included *para*-methoxyamphetamine, *para*-  
31 methoxymethamphetamine, 4-methylthioamphetamine, *N*-methyl-benzodioxolylbutanamine,  
32 benzodioxolylbutanamine, 5-(2-aminopropyl)benzofuran and 6-(2-aminopropyl)benzofuran.  
33 Identification and structural elucidation of the metabolites was performed using liquid  
34 chromatography-quadrupole-time-of-flight mass spectrometry. The targeted drugs were  
35 mainly metabolised by cytochrome P450 enzymes via *O*-dealkylation as the major pathway,  
36 followed by *N*-dealkylation, oxidation of unsubstituted C atoms and deamination (to a small  
37 extent). These drugs were largely free from Phase II metabolism. Only a limited number of  
38 metabolites were found which was consistent with the existing literature for other  
39 phenethylamine-based drugs. Also, the metabolism of most of the targeted drugs progressed  
40 at slow rate. The reproducibility of the identified metabolites was assessed through  
41 examining formation patterns using different incubation times, substrate and enzyme  
42 concentrations. Completion of the work has led to a set of metabolites which are  
43 representative for specific detection of these drugs in intoxicated individuals and also for  
44 meaningful evaluation of their use in communities by wastewater-based drug epidemiology.  
45

46 **Keywords:** new psychoactive substances, metabolite characterisation, high-resolution mass  
47 spectrometry, wastewater-based epidemiology, LC-QTOF-MS analysis

48 Word count

Abstract	228
Main text	6774
Total no. of words	7002
No. of tables	4
No. of figures	6

49

50

## 51 1. Introduction

52 In recent years, there has been a clear increasing trend in the production and use of new  
53 psychoactive substances (NPS), internationally [1]. NPS are considered as substances that are  
54 not under the control of the 1961 Single Convention on Narcotic Drugs or the 1971  
55 Convention on Psychotropic Substances but which may pose a threat to public health [1-3].  
56 There are many different families of NPS, such as phenethylamines, cathinones, piperazines,  
57 and synthetic cannabinoids [2]. In the global NPS market, the number of phenethylamine  
58 derivatives was ranked as the second highest and accounted for about 23% of the total  
59 number of reported NPS in 2009–2012 [2]. To circumvent legislative band, these  
60 phenethylamine-based designer drugs are typically chemically modified from the molecular  
61 structure of classical phenethylamine-based illicit drugs, such as amphetamines and 3,4-  
62 methylenedioxymethamphetamine (MDMA), and still maintain amphetamine- and/or  
63 MDMA-like physiological effects. The description of a substance as an NPS does not  
64 necessarily mean it is an entirely novel substance, but can also reflect recent increased  
65 availability on the drug market [1-3]. For instance, *para*-methoxymethamphetamine  
66 (PMMA), first synthesised in the late 1930s, emerged on the drug market in 2011-2013 and  
67 then appeared again recently causing several fatal intoxication cases in England, the  
68 Netherlands and Australia [4-6].

69 Identification of NPS and their specific metabolites in human samples (e.g. serum, urine  
70 and/or saliva) is critical in forensic and clinical toxicology for provision of intoxication  
71 evidence. Also, research related to determining NPS metabolites is beneficial to the emerging  
72 field of wastewater-based drug epidemiology, in which specific drug metabolites are  
73 measured in wastewater to back-estimate the use of these substances in communities [7, 8]. A  
74 few recent studies have analysed raw wastewater samples for some phenethylamine-based  
75 designer drugs to understand their use in the communities [9-13]. Monitoring metabolised  
76 drug residues in addition to the parent drug could improve efforts to determine the extent of

77 the population use of these substances, especially when the parent drug concentrations in  
78 wastewater are low or below the sensitivity of analytical methods.

79 Due to the ethical limitation on studying *in vivo* drug metabolism in humans, an *in vitro*  
80 approach has been proposed to offer a relatively efficient and direct alternative [14]. The  
81 approach usually involves: (a) incubation of the NPS of interest with pooled human liver  
82 microsomes (HLM) for an overview of metabolism (rather than particular types of  
83 isoenzymes to understand specific metabolic processes); (b) using high resolution mass  
84 spectrometry (HRMS) to screen for all metabolites of the selected NPS; (c) elucidation of the  
85 structure of individual metabolites based on its accurate mass, MS/MS fragmentation,  
86 isotopic patterns and values of double bond equivalent. Liquid chromatography (LC)  
87 combined with HRMS such as quadrupole-time-of-flight MS (QTOF-MS) has been  
88 recognised as one of the most robust and widely applied techniques for identifying drug  
89 metabolites in *in vivo* and *in vitro* matrices, facilitating discovery of NPS metabolites [15,  
90 16]. Together, LC-HRMS with careful *in vitro* experimental designs such as using multiple  
91 incubation time points, repeating the experiments and/or using individual enzyme families to  
92 assess specific (groups of) metabolites, the reliability of the *in vitro* metabolism data can be  
93 enhanced.

94 This study selected seven phenethylamine-based designer drugs, including *para*-  
95 methoxyamphetamine (PMA), PMMA, 4-methylthioamphetamine (4-MTA), *N*-methyl-  
96 benzodioxolylbutanamine (MBDB), benzodioxolylbutanamine (BDB), 5-(2-  
97 aminopropyl)benzofuran (5-APB) and 6-(2-aminopropyl)benzofuran (6-APB) (Fig. 1) to  
98 assess its human *in vitro* metabolism. These drugs are commonly considered as NPS, except  
99 for PMA and 4-MTA which were listed on the 1971 Convention on Psychotropic Substances  
100 as of September 2013. Also, a few of them including MBDB, 4-MTA and PMMA have been  
101 included in the Risk Assessment Reports of the European Monitoring Centre for Drugs and  
102 Drug Addiction [17]. The rationale for this study is based on the fact that there is a lack of a

103 clear understanding of human *in vitro* metabolites for these drugs; as previous related *in vitro*  
104 studies have been limited to a focus on understanding what types of isoenzymes participate in  
105 specific metabolism processes [18-23], and also that there have been no studies performed for  
106 the screening and structural elucidation of potential *in vitro* metabolites of these drugs using  
107 LC-HRMS. Furthermore, no comparisons of human *in vitro* metabolism for these drugs,  
108 which are closely related in structure, have ever been made under the same experimental  
109 conditions.

110 Therefore, the main objective of this study was to screen for potential *in vitro*  
111 metabolites of these designer drugs to be formed in HLM using untargeted analysis with LC-  
112 QTOF-MS. Hence, HLM as an enzyme cocktail was applied, instead of selected types of  
113 isoenzymes [18-23], to generate all the possible cytochrome P450 metabolites. Also, this  
114 study aimed to assess the *in vitro* metabolism of these drugs in a stepwise experimental  
115 design with individual enzyme family preparations, and to characterise their potential  
116 metabolites, propose and compare their respective metabolic pathways.

117

## 118 **2. Materials and methods**

### 119 **2.1. Chemicals and reagents**

120 Chemical standards for PMA, PMMA, 4-MTA, MBDB, BDB, 5-APB and 6-APB were  
121 obtained from LGC Standards SARL (Molsheim, France) and Cerilliant (Round Rock, Texas,  
122 USA) at the concentration of 1 mg/mL in methanol or acetonitrile. The internal standard,  
123 theophylline, was obtained as powder (anhydrous, purity>99%) from Sigma-Aldrich  
124 (Diegem, Belgium). Pooled human liver microsomes (HLM; mix gender, n=50) were  
125 purchased from Tebu-bio (Boechout, Belgium). Pooled human liver cytosol (HLCYT; mix  
126 gender, n=50), chemical standards for 2,6-uridinediphosphate glucuronic acid (UDPGA),  
127 alamethicin (neat, purity>99%), 3'-phosphoadenosine-5'-phosphosulfate (PAPS; neat,  
128 purity>60%) lithium salt hydrate, 4-nitrophenol (4-NP), 4-nitrophenol-glucuronide (4-NP-

129 Gluc; neat, purity>99%), 4-nitrophenol-sulfate (4-NP-Sulf; neat, purity>99%), naphthol-  
130 glucuronide (Naphth-Gluc; neat, purity>99%), 5-bromo-4-chloro-3-indolyl sulfate (Indolyl-  
131 Sulf; neat, purity>99%) and NADPH (neat, purity>99%) were purchased from Sigma-  
132 Aldrich (Diegem, Belgium). Ultrapure water was prepared using a Purelab flex water system  
133 by Elga (Tienen, Belgium). Acetonitrile, methanol, ammonium hydroxide, hydrochloric acid  
134 and ammonium acetate were purchased from Merck (Darmstadt, Germany). All organic  
135 solvents were HPLC grade or higher.

## 136 **2.2. Tiered approaches on *in vitro* drug metabolism**

137 In this study, a two-tiered approach for investigating Phase I and Phase II *in vitro* drug  
138 metabolism was followed (Fig. 2). The purpose of tier I was to screen for the major  
139 metabolites formed and the family of enzymes involved in their formation, in a similar  
140 manner to the typical practice for *in vitro* metabolism studies. Tier I consisted of two parts,  
141 tier-IA and -IB. In tier IA, a direct metabolism of the drugs of interest was investigated, in  
142 which Phase I metabolites and direct Phase II metabolites of the parent drug (when possible  
143 to be formed) were screened. This allowed investigation of direct drug metabolism mediated  
144 separately by Phase I and Phase II enzymes. After that, tier IB was employed to investigate  
145 the Phase II metabolism of Phase I metabolites detected in tier IA, providing information on  
146 the formation of secondary metabolites. Tier II aimed to assess the consistency and  
147 reproducibility of the metabolite formed in tier I and to determine the major, intermediate and  
148 minor metabolites by monitoring over various incubation times (10, 20, 40, 60, and 90 min),  
149 enzyme concentrations (0.2, 0.4, 0.6, and 0.8 mg/mL) and substrate concentrations (1, 3, 5,  
150 and 10  $\mu$ M).

## 151 **2.3. *In vitro* drug metabolism assays**

152 For tier IA samples focusing on cytochrome P450 (CYP) enzymes, the reaction mixture  
153 (final volume: 1 mL), consisting of 100 mM phosphate buffer (pH 7.4), HLM (final  
154 concentration: 0.5 mg/mL) and the substrate (final concentration: 10  $\mu$ M) was pre-incubated



155 for 5 min in a shaking water bath at 37 °C. The reaction was initiated by addition of 10 µL of  
156 NADPH solution (final concentration: 1 mM) in the phosphate buffer. To keep the NADPH  
157 concentration saturated, an extra aliquot was added every hour. To stop the reaction after 2 h,  
158 250 µL of an ice-cold acetonitrile solution containing 1% formic acid and 5.0 µg/mL of  
159 theophylline (used as internal standard) was added to each sample, which was then vortex-  
160 mixed for 30 s and centrifuged at 8,000 rpm for 5 min. The supernatant was then transferred  
161 to a glass tube, and concentrated to 200 µL under a gentle stream of nitrogen gas at 60 °C. A  
162 20 µL aliquot of acetonitrile was then added to the extract before transferring it to a HPLC  
163 vial for analysis. For tier IA samples focusing on uridinediphosphate glucuronic acid  
164 transferase (UGT) enzymes, the reaction mixture was prepared as described above for CYP  
165 enzyme samples, but adding a 10 µL aliquot (final concentration: 10 µg/mL) of alamethicin  
166 (for opening the pore of microsomal inner lumen, where UGTs are expressed) dissolved in  
167 dimethyl sulfoxide before pre-incubating the samples in the water bath. Also, the cofactor  
168 UDPGA was used instead of NADPH, but at the same final concentration (1 mM). An aliquot  
169 of UDPGA was added to the reaction mixture every hour, similarly to NADPH in the CYP  
170 experiments. In tier IA samples focusing on sulfotransferase (SULT) enzymes, the reaction  
171 mixture was prepared as described above for CYP enzyme samples, but using HLCYT (final  
172 concentration: 0.5 mg/mL) instead of HLM and using PAPS instead of NADPH as the  
173 cofactor at the same final concentration (1 mM). An aliquot of PAPS was added to the  
174 reaction mixture every hour. Samples were then processed as described above for CYP  
175 enzyme samples.

176 In tier IB, formation of glucuronidated and sulfated metabolites of the Phase I  
177 metabolites produced in tier IA experiments was investigated in two major steps. First, Phase  
178 I metabolites of the drug of interest were enzymatically produced as described in tier IA for  
179 three hours. The reaction was quenched by keeping the samples on ice for 5 min, followed by  
180 centrifugation at 8,000 rpm for 5 min. Then, 940 µL of the supernatant, containing the

181 fraction of parent drug and its metabolites generated by CYP enzymes, was transferred to a  
182 new tube which contained a fresh aliquot of pooled HLM or HLCYT (final concentration: 0.5  
183 mg/mL) for the samples investigating UGT or SULT mediated metabolism, respectively.  
184 Alamethicin and the appropriate cofactors were added at the concentrations and time intervals  
185 described above for tier IA samples. The samples were incubated for two hours and prepared  
186 as described above.

187 In the tier II experiments, three different sets of samples were prepared. In the first set,  
188 the reaction mixture (1 mL) consisted of 100 mM phosphate buffer, pooled HLM (0.8  
189 mg/mL) and the substrate (10  $\mu$ M). The reaction was initiated by addition of NADPH, and  
190 stopped after 10, 20, 40, 60, and 90 min. In the second set, the reaction mixture consisted of  
191 100 mM phosphate buffer, pooled HLM at different total protein concentrations (final  
192 concentrations: 0.2, 0.4, 0.6, and 0.8 mg/mL) and a constant concentration of the substrate  
193 (10  $\mu$ M). The reaction was initiated by addition of NADPH and was stopped after 90 min. In  
194 the third set, the reaction mixture consisted of 100 mM phosphate buffer, pooled HLM at a  
195 constant protein concentration (0.8 mg/mL) and the substrate at different concentrations (final  
196 concentrations: 1, 3, 5, and 10  $\mu$ M). The reaction was initiated by addition of NADPH and  
197 was stopped after 90 min. The reaction was quenched and the samples were prepared as  
198 described in tier IA section above.

199 Positive and negative control samples for each family of enzymes of interest were  
200 routinely prepared. In the positive control samples for UGT and SULT activity, 4-nitrophenol  
201 was selected as the substrate and the formation of 4-nitrophenol-sulfate and 4-nitrophenol-  
202 glucuronide, respectively, was monitored. Samples were prepared as described in the tier IA  
203 section above. No positive control samples for CYP activity were prepared, because data  
204 about the catalytic activity of major human liver CYPs was provided by the HLM vendor.  
205 Three different negative control samples were prepared by omitting the enzymes, the

206 substrate, or the cofactor in the reaction mixture. The negative control samples for CYP,  
207 UGT and SULT activity were prepared as described in tier I section above.

#### 208 **2.4. LC-QTOF-MS analysis**

209 Samples were analysed by a LC-QTOF-MS system which consisted of a 1290 Infinity  
210 LC (Agilent Technologies) connected to a 6530 Accurate-Mass QTOF-MS (Agilent  
211 Technologies). Chromatographic separation of the extracts was achieved using a C<sub>8</sub> Zorbax  
212 Eclipse Plus column (150 X 2.1 mm, 3.5 µm, Agilent Technologies) with a mobile phase  
213 composition of 5 mM ammonium acetate in ultrapure water (A) and acetonitrile (B) at 40°C.  
214 The gradient program was as follows: 2% B for the first 5 min followed by linear increase of  
215 B from 2 to 22% from 5 to 25 min and from 22 to 80% from 25 to 26 min. Solvent B was  
216 maintained at 80% for 4 min, decreased to 2% from 30 to 30.5 min and kept at 2% from 30 to  
217 40 min to re-equilibrate the column. The total run time was 40 min per sample. The flow rate  
218 was 0.2 mL/min with an injection volume of 2 µL.

219 The acceptable mass accuracy (within ±2 ppm) of the QTOF-MS was calibrated before  
220 each analysis using a reference solution for scanning up to 1700 mass-to-charge ratio ( $m/z$ )  
221 with extended dynamic range (2 GHz). Samples were analysed using positive and negative  
222 electrospray ionisation (+/-ve ESI) modes individually, with the fragmentor voltage at 300 V  
223 and gas temperature 325 °C. The QTOF-MS was set to acquire  $m/z$  ranging between 50 and  
224 1000 amu at a scan rate of 2.5 spectra per s (i.e. 400 ms/spectrum). The auto-MS/MS function  
225 was used to obtain MS/MS spectra of precursor ions using three different collision energies  
226 (10, 20 and 40 eV). Precursor ions were targeted if ion abundances exceeded the threshold of  
227 2000 with a maximum of three precursor ions per cycle.. The QTOF-MS was set to scan  
228 MS/MS  $m/z$  from 50 to 500 amu. To avoid over-fragmentation of the same precursor ion, an  
229 active exclusion function was set to exclude the precursor ions after every two spectra and  
230 release it after 0.2 min. During analysis, the reference mass standard solution (commercially  
231 available from Agilent) was constantly infused onto the QTOF-MS for monitoring and

232 measuring its mass accuracy with the reference masses of 121.0508 and 922.0097 for +ve  
233 ESI and of 119.0352 and 980.0152 for -ve ESI.

## 234 **2.5. Data analysis**

235 Two different approaches were used to assist the interpretation of the potential *in vitro*  
236 metabolites formed. For approach 1, potential Phase I metabolites were predicted based on  
237 authors' knowledge considering (a) the molecular structure of the drug, (b) the family of  
238 enzymes that might be able to metabolise it and (c) the type of reactions that these families of  
239 enzymes are known to catalyse. Once the Phase I metabolites were experimentally  
240 determined (tier IA experiments), the families of Phase II enzymes that might be able to  
241 further metabolise them were identified and the structures of the Phase II metabolites were  
242 predicted. For approach 2, possible metabolites were estimated using metabolism-specific  
243 software (Nexus v1.5, Lhasa Limited), in which the chemical structure of the drug, the  
244 species of interest (i.e. humans), the enzyme families and a minimum likelihood of metabolite  
245 formation (i.e. "equivocal") were used for prediction. The prediction was conducted up to  
246 tertiary metabolites and for a maximum of 100 metabolites. The two approaches were  
247 independently applied to the same acquired raw data file, allowing determinations of their  
248 consistency, for better understanding the potential *in vitro* metabolites generated. The  
249 approach of data analysis has been previously applied in our team for assessing human *in*  
250 *vitro* metabolism of environmental contaminants [24, 25] and also recently shown feasible for  
251 evaluating *in vitro* data on human drug metabolism with *in silico* methods[26].

252 The chromatographic features of each compound, such as the retention time and peak  
253 area counts, were obtained from the extracted ion chromatograms. To confirm the  
254 identification of a metabolite, the following criteria were applied: (a) the measured molecular  
255 *m/z* of the precursor ion and the product ions should be respectively within 10 and 25 ppm of  
256 its theoretical value (higher mass tolerances taken into account lower sensitivities with small  
257 amounts of product ions); (b) the isotopic patterns should be overlaid at least 75% with the

258 predicted ones; (c) the measured double bond equivalent (DBE) value should match with the  
259 postulated structure; (d) the absence of the possible metabolite at the same retention time in  
260 all the negative control samples; (e) the proposed chemical structure of the detected  
261 metabolite has to be logical considering the chemical structure of the substrate and the  
262 reactions that the family of enzymes under investigation is able to catalyse; and (f) the  
263 retention time of the detected metabolites should not be higher than that of the parent drug.  
264 Tier II data are presented as the response value, which was calculated as the peak area ratio of  
265 the metabolite or the parent drug to the internal standard (theophylline) for compensating  
266 inter-sample and instrumental variability during analysis.

267

### 268 3. Results

#### 269 3.1. PMA and PMMA

270 In tier IA samples, the only metabolite of PMA detected was formed via *O*-  
271 demethylation catalysed by CYP enzymes, resulting in a *para*-hydroxylated metabolite  
272 (PMA-M1) (Table 1 and Fig. 3A). Its molecular ion was  $m/z$  152.1063 with the difference in  
273 mass error between the measured and theoretical mass (i.e.  $\Delta_{\text{mass}}$ ) at +4.60 ppm and the  
274 measured DBE value at 4 (Table 1). With different collision energy values applied (Fig. S1),  
275 the molecular structure of PMA-M1 was elucidated through five potential major fragment  
276 ions which were  $m/z$  135.0799, 107.0495, 91.0552, 77.0390 and 65.0364 (Table 1, Fig. S1).  
277 The fragment ion  $m/z$  135.0799 resulted from a loss of  $\text{NH}_3$  and then was further fragmented  
278 with a loss of  $\text{C}_2\text{H}_4$  (ethylene) to yield  $m/z$  107.0495 ( $\text{C}_7\text{H}_7\text{O}^+$ ). The ion  $\text{C}_7\text{H}_7\text{O}^+$  is likely a  
279 hydroxyl-tropylium ion which possibly facilitates the loss of the hydroxyl group on the  
280 benzyl moiety. The fragment ions  $m/z$  91.0552 ( $\text{C}_7\text{H}_7^+$ , benzylium ion  $\leftrightarrow$  tropylium ion),  
281 77.0390 ( $\text{C}_6\text{H}_5^+$ , radical benzene) and 65.0364 ( $\text{C}_5\text{H}_5^+$ , a loss of  $\text{CH}\equiv\text{CH}$  from tropylium  
282 ion) represent the hallmark features of the alkylbenzene moiety [27]. Also, PMA-M1 eluted  
283 approximately 10 min earlier than the parent compound, suggesting that it has a higher

284 polarity than PMA, in agreement with the formation of a hydroxylated metabolite. PMA-M1  
285 was not detected in any of the three negative control samples, confirming it to be a metabolite  
286 produced by CYP enzymes.

287 In tier IA samples, two metabolites of PMMA were detected (Table 2). The precursor ion  
288 of the first metabolite (PMMA-M1) was  $m/z$  166.1234 with the measured DBE value at 4,  
289 corresponding to the metabolite resulting from *O*-demethylation of PMMA catalysed by  
290 CYPs ( $\Delta_{\text{mass}} = +4.82$  ppm) (Table 2, Fig. 3B). The pattern of the MS/MS spectrum of  
291 PMMA-M1 was like that of PMA, suggesting the presence of a hydroxylated group in the  
292 *para* position of PMMA-M1 as well. The major fragments of PMMA-M1 included the loss of  
293  $\text{NH}_2\text{CH}_3$  for  $m/z$  135.0798 and the loss of  $\text{NH}_2\text{CH}_3$  and  $\text{CH}_4$  for  $m/z$  119.0472 (Table 2, Fig.  
294 S2A). The presence of the alkylbenzene moiety was noticed at  $m/z$  107.0483, 91.0540,  
295 77.0383 and 65.0380 (see above). The precursor ion of the second metabolite (PMMA-M2)  
296 of PMMA was  $m/z$  166.1208 ( $\Delta_{\text{mass}} = +10.8$  ppm) and the measured DBE value at 4 (Table  
297 2), which represented the metabolite produced by *N*-demethylation of PMMA by CYP  
298 enzymes (Fig. 3B). The structure of PMMA-M2 can be explained by three major product ions  
299 and the feature of the alkylbenzene moiety (Table 2, Fig. S2B). A loss of  $\text{NH}_3$  for  $m/z$   
300 149.0931 remained the common fragment. This ion was further fragmented with a loss of  
301  $\text{CH}_4$  and  $\text{C}_2\text{H}_4$  for the product ions  $m/z$  135.0790 and 121.0625, respectively. Both PMMA-  
302 M1 and PMMA-M2 eluted several min earlier than PMMA, suggesting that they are more  
303 hydrophilic compounds than PMMA, which is consistent with their postulated structures.  
304 Furthermore, the retention time of PMMA-M2 was same as that of the PMA standard, which  
305 further substantiates its structural identification. Both PMMA-M1 and PMMA-M2 were not  
306 detected in any of the three negative control samples, confirming that both PMMA  
307 metabolites were produced by CYP enzymes.

308 Conjugated metabolites of PMA, PMMA and of their CYP-mediated metabolites (i.e.  
309 PMA-M1, PMMA-M1 and PMMA-M2) were not detected either in tier IA, nor tier IB

310 samples. However, in the positive control samples, 4-NP-GLUC and 4-NP-SULF,  
311 metabolites of 4-NP produced by UGTs and SULTs, respectively, were detected. This result  
312 suggests that the experiment was conducted properly and that both UGTs and SULTs  
313 expressed normal catalytic activity. Therefore, the positive control samples substantiated the  
314 lack of formation of glucuronidated and sulfated metabolites of PMA-M1, PMMA-M1 and  
315 PMMA-M2 under the experimental conditions tested.

316 PMA-M1 was consistently detected in all tier II samples and not in any of the negative  
317 control samples. There was a clear increasing trend of formation of PMA-M1 with incubation  
318 times, protein concentrations and substrate concentrations (Figs. 4A-C). This confirmed that  
319 PMA-M1 was a metabolite of PMA produced by CYPs. The formation trend of PMA-M1  
320 appeared linked with the reduction of PMA (Figs. 4A-B), providing further evidence of the  
321 biotransformation of PMA to PMA-M1.

322 Similarly, both metabolites of PMMA identified in tier IA were also detected in the tier  
323 II samples. The amount of both PMMA-M1 and PMMA-M2 increased with the incubation  
324 time, protein concentrations and substrate concentrations (Figs. 4D-F), confirming that  
325 PMMA-M1 and PMMA-M2 were the metabolites of PMMA produced by CYP enzymes. In  
326 contrast, the parent compound showed an opposite (decreasing) trend. Also, under the  
327 different incubation conditions used, PMMA-M1 was formed faster than PMMA-M2 (Figs.  
328 4D-F), suggesting that PMMA-M1 was the primary *in vitro* metabolite of PMMA. Both  
329 PMMA-M1 and PMMA-M2 were not detected in any of the three negative control samples,  
330 confirming that they were metabolites of PMMA, formed by CYP enzymes. The two data  
331 analysis approaches provided consistent results.

### 332 3.2. 4-MTA

333 In tier IA samples, four metabolites (4-MTA-M1, -M2, -M3 and -M4) formed by CYP  
334 enzymes were detected (Table 3). None of the four metabolites were detected in any of the  
335 three negative control samples. The 4-MTA-M1 precursor ion was  $m/z$  198.0946 ( $\Delta\text{mass} = -$

336 0.50 ppm) and the measured DBE value at 4, representing a hydroxylated metabolite of 4-  
337 MTA (Fig. 3C). The structure of 4-MTA-M1 was further elucidated by its MS/MS spectrum  
338 (Table 3, Fig. S3A). The loss of  $\text{NH}_3$  and  $\text{NH}_2\text{CH}_2\text{CH}_3$  gave the product ions  $m/z$  181.0674  
339 and 153.0362 respectively. The loss of  $\text{NH}_3$  followed by that of  $\text{CH}_3\text{SH}$  from the molecule  
340 facilitated the equilibrium moiety between ketone and hydroxyl-ethylene for the fragment ion  
341  $m/z$  133.0639. This was likely to further break the OH and C=C bond readily to produce the  
342 fragment ion  $m/z$  117.0690 and 107.0490, respectively. The characteristic fragment ions for  
343 the alkylbenzene moiety were identified at  $m/z$  91.0544, 77.0382 and 65.0391. The fragment  
344 ions  $m/z$  133.0639 and 107.0490 provided consistent evidence that the hydroxyl group was  
345 located on the alkyl chain rather than on the benzyl ring of 4-MTA. Also, 4-MTA-M1 eluted  
346 about 16 min earlier than 4-MTA, suggesting it was a more polar compound than 4-MTA,  
347 which is consistent with its postulated structure. The precursor ion of 4-MTA-M2 was  $m/z$   
348 168.0836 ( $\Delta_{\text{mass}} = -2.97$  ppm) with the measured DBE value at 4, matched to a thiol  
349 metabolite resulting from *S*-demethylation of 4-MTA (Table 3). The structure of 4-MTA-M2  
350 was postulated by the product ions  $m/z$  151.0558 possibly due to the loss of  $\text{NH}_3$ , 117.0692  
351 likely due to the loss of  $\text{NH}_3$  and  $\text{SH}_2$ , and 91.0536 resulting from the formation of  
352 benzylium/tropylium ion (Table 3, Fig. S3B). Also, 4-MTA-M2 eluted about 13 min earlier  
353 than 4-MTA (Table 3), suggesting that it is a more polar compound than the substrate.

354 The 4-MTA-M3 precursor ion was  $m/z$  197.0633 ( $\Delta_{\text{mass}} = +1.01$  ppm) with a measured  
355 DBE value of 5, and this matched to the metabolite resulting from oxidative deamination of  
356 4-MTA-M1 by CYPs (Table 3, Fig. 3C). The structure of 4-MTA-M3 was postulated by the  
357 fragment ion  $m/z$  197.0631 (Table 3, Fig. S3C). The acyloin function group,  $\alpha$ -hydroxyl  
358 ketone, was readily broken to yield the fragment ion  $m/z$  137.0411. After that, the fragment  
359 ions  $m/z$  122.0184 and 121.0095 corresponded to the potential resonance double and triple  
360 bonding between the S and C atom [28]. The fragment ions for the alkylbenzene moiety of



361 the 4-MTA-M3 molecule were noticed (Table 3). 4-MTA-M3 eluted about five min later than  
362 4-MTA-M2 (Table 3), suggesting it is a less polar compound than 4-MTA-M2.

363 The 4-MTA-M4 precursor ion was  $m/z$  199.0787 with the measured DBE value at 4  
364 (Table 3, Fig. S3D), corresponding to a di-hydroxylated metabolite of 4-MTA from reduction  
365 of 4-MTA-M3 (Fig. 3C). The molecular structure of 4-MTA-M4 was similar to that of 4-  
366 MTA-M1 and 4-MTA-M3, as suggested by the common fragment ions present in the MS/MS  
367 profiles of these three compounds (Fig. S3). For example, the cleavage of the OH-C=C-OH  
368 and the rearrangement of the C-S bond led to the fragment ions  $m/z$  122.0156, 121.0097 and  
369 107.0491. The loss of SHCH<sub>3</sub> from the benzene ring and the dihydroxylated group gave the  
370 fragment ion  $m/z$  117.0712, which was then further fragmented to form benzylium/tropylium  
371 ion  $m/z$  91.0547 and the related radical benzene  $m/z$  77.0375. 4-MTA-M4 eluted about 6 min  
372 earlier than 4-MTA, suggesting it is a more polar compound of 4-MTA due to the addition of  
373 two hydroxylated groups.

374 Phase II metabolites of 4-MTA and their CYP-mediated metabolites (i.e. 4-MTA-M1, -  
375 M2, -M3 or -M4) were not detected neither in tier IA nor tier IB samples, whereas 4-NP-  
376 GLUC and 4-NP-SULF were found in the UGT and SULT positive control samples,  
377 respectively. The positive results from the positive control samples supported the lack of  
378 formation of glucuronidated and sulfated metabolites of 4-MTA-M1, -M2, -M3 and -M4  
379 under the experimental conditions used.

380 In tier II samples, 4-MTA-M1, -M3 and -M4, but not -M2, were detected. These  
381 metabolites were not detected in any of the three negative control samples. The formation of  
382 4-MTA-M1, -M3 and -M4 increased with incubation time, protein concentration and  
383 substrate concentration values used (Fig. 5). In all the analysed samples, 4-MTA-M1 was  
384 consistently formed more quickly than 4-MTA-M4, followed by 4-MTA-M3. This result  
385 suggested that 4-MTA-M1, -M3 and -M4 were the primary, intermediate and tertiary

386 metabolite of 4-MTA, respectively, under the range of incubation conditions tested, whereas  
387 4-MTA-M2 was only a minor metabolite of 4-MTA.

### 388 **3.3. BDB and MBDB**

389 In tier IA samples, no metabolites of BDB produced by CYPs were detected. Only one  
390 metabolite of MBDB was detected (MBDB-M1). Its measured precursor ion was  $m/z$   
391 194.1174 with the DBE value at 5, which matched to the molecular ion of the *N*-  
392 demethylated metabolite of MBDB produced by CYPs ( $\Delta_{\text{mass}} = +1.03$  ppm, Table 4, Fig.  
393 3D). MBDB-M1 was not found in any of the three negative control samples, suggesting that  
394 it was a metabolite of MBDB formed by CYP enzymes. The postulated structure of MBDB-  
395 M1 was elucidated by its MS/MS profile (Table 4, Fig. S4). The loss of  $\text{NH}_3$  from MBDB-  
396 M1 ion resulted in the product ion  $m/z$  177.0894 which then results in  $m/z$  135.0447 due to  
397 the loss of the propyl group. With higher collision energy, the dioxolane ring of the MBDB-  
398 M1 was broken to form the fragment ions  $m/z$  117.0327 and 105.0329. Again, the feature of  
399 the alkylbenzene moiety with  $m/z$  107.0499, 91.0526 and 77.0391 was detected as the  
400 MS/MS fragment ions of MBDB-M1. Also, MBDB-M1 eluted approximately two min earlier  
401 than MBDB, suggesting that MBDB-M1 was slightly more polar than MBDB, consistent  
402 with its postulated structure. The retention time and the MS/MS fragmentation patterns of  
403 MBDB-M1 were as alike as that of BDB. No glucuronidated and sulfated analogues of  
404 MBDB and MBDB-M1 were detected in both tier IA and IB samples. Detection of 4-NP-  
405 GLUC and 4-NP-SULF in positive control samples substantiated the lack of formation of  
406 glucuronidated and sulfated metabolites of MBDB-M1 under the experimental conditions.

407 MBDB-M1 was detected in all tier II samples, but not found in any of the three negative  
408 control samples. No other MBDB metabolites produced by CYPs were detected, which was  
409 consistent with the results obtained in tier IA. MBDB-M1 formation increased with  
410 incubation times, protein concentrations and substrate concentrations (Fig. 6), providing  
411 further evidence that MBDB-M1 was the (only) metabolite of MBDB formed by CYPs. Since

412 no BDB metabolites produced by CYPs were identified in tier I, a tier II experiment was not  
413 conducted for BDB.

#### 414 **3.4. 5-APB and 6-APB**

415 No metabolites of 5-APB and 6-APB produced by CYP, UGT and SULT enzymes were  
416 detected in any tier I samples. Again, 4-NP-GLUC and 4-NP-SULF were respectively  
417 detected in the UGT and SULT positive control samples. Consequently, tier II experiments  
418 were not conducted.

419

#### 420 **4. Discussion**

421 This study successfully investigated the formation and characterisation of *in vitro*  
422 metabolites of seven phenethylamine-based designer drugs using HLM and LC-QTOF-MS.  
423 In tier IA, structures of the possible metabolites were predicted through interpreting the  
424 potential enzymatically-catalysed reactions between the parent drug and the family of  
425 enzymes selected. Since reference standards for the CYP-produced metabolites detected in  
426 tier IA may not be always available from commercial laboratories, the current study included  
427 tier IB experiments, in which these primary metabolites were enzymatically generated and  
428 then incubated with the enzyme mixture containing the Phase II enzyme families (i.e. UGTs  
429 and SULTs). Furthermore, this study presented tier II experiments as an extended approach to  
430 confirm the metabolites identified in tier I, by understanding the formation profiles of the  
431 metabolites according to three different experimental conditions. With such multiple testing  
432 conditions, the work overall provides a comprehensive assessment of the *in vitro* experiments  
433 for higher reproducibility and consistency of *in vitro* metabolism data. It should be noted that  
434 careful attention has been paid to the preparation of the reaction mixture in this study:  
435 particularly, (a) the organic solvent content was kept at maximum 1% of the reaction mixture  
436 to minimise its dose-dependent impact on the enzyme catalytic activity [29, 30]; (b) the  
437 NADPH was replenished every hour to counterbalance its deterioration over time and to thus

438 maintain its concentration close to saturation [31]; (c) the final protein concentration in each  
439 sample was kept below 1 mg/mL to avoid large extents of non-specific protein binding of the  
440 substrate [32, 33]; (d) a three-hour long incubation was conducted in tier IB to generate  
441 enough Phase I metabolites for further Phase II reactions (Fig. 2); (e) positive and negative  
442 control samples were prepared as quality controls of the experiments for justifying the  
443 obtained results; (f) theophylline (which ionises in both positive and negative modes) was  
444 chosen as the internal standard to compensate variations during sample preparation and  
445 analytical measurements.

446 This study showed that the *in vitro* metabolism of PMA and PMMA was relatively slow,  
447 with only one metabolite (*para*-hydroxyamphetamine) formed from PMA and two  
448 metabolites (primary: *para*-hydroxymethamphetamine; secondary: PMA) from PMMA. As  
449 they share a phenethylamine moiety, the proposed pathway of PMA and PMMA metabolism  
450 in the present study was in agreement with that of other illicit phenethylamine drugs. For  
451 example, both amphetamine and methamphetamine are not extensively metabolised in  
452 humans (about 30% and 40% of the parent compound is measured in human urine,  
453 respectively) [34]. The primary metabolite of PMA and PMMA (PMA-M1 and PMMA-M1,  
454 respectively) was mainly produced by CYP-mediated *O*-demethylation. However, this  
455 reaction occurred approximately 10 to 20 times faster for PMMA than for PMA, which was  
456 observed consistently with increasing experimental times, enzyme concentrations, and  
457 substrate concentrations (see red symbols in Fig. 4). Since the structural difference between  
458 PMA and PMMA is only the methylation of the amino group (for PMMA), the obtained data  
459 suggest that the presence of the methylated amino group substantially favoured an *O*-  
460 dealkylation metabolism pathway to produce *para*-hydroxyl metabolites. Similar results were  
461 also obtained in previous studies when comparing amphetamine and methamphetamine *in*  
462 *vivo* metabolism in humans. While the *para*-hydroxyl metabolite is common for  
463 amphetamine and methamphetamine, its formation is more pronounced for methamphetamine

464 than amphetamine (15% vs. 3%, respectively) [34-36]. Moreover, the *in vitro* metabolism of  
465 PMMA investigated in this study showed that the *N*-dealkylation reaction was about five to  
466 seven times less favourable than the *O*-dealkylation (see red and purple symbols in Figs. 4D-  
467 F). This is consistent with *N*-demethylation of methamphetamine to amphetamine (about 4-  
468 7% of a methamphetamine dose excreted in urine), occurring only to a very small extent [34].

469 The metabolites of PMA and PMMA detected in this study are generally consistent with  
470 those reported in the literature. PMA-M1 was the major *in vitro* metabolite produced by  
471 CYP2D6 [18] and the major *in vivo* metabolite in urine samples of three healthy volunteers  
472 who consumed PMA [37, 38] (Table S1). Similarly, CYP2D6 has been found to mediate the  
473 *in vitro* formation of PMMA-M1 in humans [19, 20, 38]. To our knowledge, *in vivo*  
474 metabolism studies of PMMA are not available for humans, only for rats [39]. In urine  
475 samples collected from rats administered with PMMA, PMMA-M1 and PMMA-M2 were the  
476 major and the minor metabolites detected, respectively (Table S1). This result is in agreement  
477 with the *in vitro* data of this study, implying a common metabolism pathway of PMMA in  
478 rats and humans.

479 Glucuronidated PMA-M1 was occasionally detected in the urine samples of the three  
480 volunteers [37] (Table S1). For glucuronidated and/or sulfated metabolites of PMMA, minor  
481 amounts were found in the rat urine [39] (Table S1). Similarly, urinary excretion of  
482 conjugated metabolites for amphetamine and methamphetamine was observed only to a small  
483 extent in humans [34-36]. Taken together, these findings consistently reveal that *in vivo*  
484 glucuronidation and sulfation is not a major part of the metabolic pathway of PMA and  
485 PMMA in humans and rats. This finding is coherent with the lack of detection of PMA and  
486 PMMA Phase II metabolites in the *in vitro* metabolism experiments of this study.

487 This study revealed that 4-MTA was largely metabolised into four metabolites (Table 3)  
488 and a clear trend of their formation was observed (Fig. 5). The results also suggest that the  
489 mechanism of the CYP-mediated metabolism of 4-MTA is different from that of PMA and

490 PMMA. The primary metabolite (4-MTA-M1) of 4-MTA is a mono-hydroxylated metabolite  
491 (4-methylthiocathine), most likely formed by oxidation of an unsubstituted C atom, catalysed  
492 by CYPs. In spite of sharing similar chemical structures among 4-MTA, PMA and PMMA,  
493 this mono-hydroxylated metabolite was not detected for PMA or PMMA. This implies that  
494 the presence of the S atom in 4-MTA at the *para* position of the phenethylamine-based  
495 chemical structure favours such oxidative metabolism rather than the O atom in PMA and  
496 PMMA. To a dealkylation reaction for such *para*-substituted phenethylamine compounds, the  
497 obtained data reveal that with CYP enzymes, *S*-dealkylation is much less favourable than *O*-  
498 dealkylation reaction. This was observed from the result that the *S*-demethylated metabolite  
499 (4-MTA-M2) of 4-MTA was only detected after the three-hour long incubations (the first set  
500 of tier IB), whereas the *O*-demethylated metabolite of PMA and PMMA were readily  
501 generated after 10 min (Fig. 4). The tier II data of 4-MTA provided an indication that 4-  
502 MTA-M1 is transformed by CYPs to the corresponding ketone (4-MTA-M3, secondary or  
503 intermediate metabolite) through an oxidative deamination (Fig. 3C). It is then reduced to a  
504 di-hydroxylated metabolite (4-MTA-M4, tertiary metabolite, Fig. 3C), showing a similar  
505 metabolism pattern to 4-MTA-M1 (see red and green symbols in Fig. 5).

506 Even less is known about 4-MTA metabolism than that for PMA and PMMA. 4-  
507 Methylthiobenzoic acid was reported as the major metabolite when incubating 4-MTA with  
508 human hepatocytes obtained from three volunteers [40], but this metabolite was not detected  
509 in this study. The discrepancy might be due to the lack of the enzymes for producing 4-  
510 methylthiobenzoic acid in HLM. In contrast, unchanged 4-MTA was found as the major  
511 compound in five human urine samples (Table S1) with a few minor metabolites identified  
512 which were formed via oxidative deamination followed by reduction to corresponding  
513 alcohol and degradation of the side chain to 4-methylthiobenzoic acid [41]. Metabolites of  
514 ring- and  $\beta$ -hydroxylation (4-methylthiocathine, i.e. 4-MTA-M1 in this study) were detected  
515 in the urine samples too [41]. Similar metabolites were also observed in mice urine samples

516 [42] (Table S1), including unchanged 4-MTA, 4-methylthiobenzoic acid, 4-methylthiocathine  
517 and hydroxyl-4-MTA on the aromatic ring and the methylthio-side chain; however,  
518 conjugation of these metabolites was hardly observed. While the identified *in vivo* and *in*  
519 *vitro* metabolites of 4-MTA partly agree with this and previous studies [40-42], the current  
520 study provides additional information on *in vitro* metabolism of 4-MTA using CYPs.

521 The obtained *in vitro* metabolism data on MBDB, BDB, 5-APB and 6-APB by HLM and  
522 HLCYT consistently indicate that these drugs are hardly metabolised. The only metabolite of  
523 MBDB was detected via an *N*-dealkylation reaction (MBDM-M1; Table 4, Fig. 3D). The  
524 difference in the chemical structure between MBDB and BDB is only the methylation of the  
525 amino group (for MBDB). The data again showed that dealkylation metabolism is more  
526 favourable at the amino than at the methyl group, consistent with what has been noticed for  
527 PMMA metabolism (Figs. 4D-F). The consistent formation pattern between MBDB-M1 and  
528 PMMA-M2 (see red symbols in Fig. 6 and purple symbols in Figs. 4D-F) implies that the *N*-  
529 dealkylation metabolism pathway for such phenethylamine-based designer drugs in general  
530 proceeds at a very slow pace. Furthermore, the lack of detection of any metabolites for BDB,  
531 5-APB and 6-APB reinforces the role of methylation of the amino group in favouring the *in*  
532 *vitro* metabolism for this group of drugs as this moiety is the major structural difference  
533 among them.

534 The results of this study are partially in line with other metabolism studies for these four  
535 drugs. For example, MBDB-M1 (i.e. BDB) was the major metabolite of MBDB in which  
536 CYP2B6 is supposed to mediate this *N*-demethylation metabolic pathway [21, 22]. Although  
537 the catechol metabolite of MBDB and BDB through mediation of CYP2D6 for demethylation  
538 [22, 23] was detected in the human and rat urine samples [21] (Table S1), this metabolite has  
539 been found to be unstable in the *in vitro* assays [21, 43]. The lack of detection of the catechol  
540 metabolite for MBDB and BDB in this study could be explained by this previous finding  
541 and/or because its amounts would have been too low in the *in vitro* samples for the QTOF-

542 MS detection limit. The latter reason could also explain the lack of detection of *N*-  
543 demethylated metabolite for BDB. The data obtained are consistent with the previous study  
544 showing that glucuronidated and sulfated conjugated metabolites of MBDB and BDB were  
545 not detected in the *in vitro* experiments using particular isoenzymes of human and rat [21].  
546 These results overall suggest that conjugation of MBDB and BDB appears not to be a major  
547 part of their metabolic pathway in humans. Human *in vitro* metabolism studies for 5-APB  
548 and 6-APB are very limited in the literature and thus *in vitro* metabolites of these drugs are  
549 not yet well-known so far [44]. While this study has found that the metabolism process of 5-  
550 and 6-APB was very slow, one study [45] has very recently shown similar results, in that only  
551 limited amounts of *in vitro* metabolites of 5-APB, including hydroxyl-5-APB, hydroxy-  
552 dihydro-5-APB and 3-carboxymethyl-4-hydroxy amphetamine, were yielded and its  
553 formation rate was very low. *In vivo* metabolites of 5-APB were recently reported in rat urine  
554 [45] but are not yet known in human urine (Table S1). Similar to the present *in vitro* study, 5-  
555 APB and 6-APB were not degraded by activated sludge (own unpublished data). These  
556 findings suggest that these two drugs are rather resistant to enzymatic and bacterial  
557 digestions.

558 *In vitro* metabolism data of the selected designer drugs are important for drug-related  
559 disciplines, such as forensic toxicology, since they provide key compounds useful to better  
560 identify these drugs in humans and crime scenes. Also, the results of the current study reveal  
561 potential human biomarkers of the targeted designer drugs to be measured in urine from  
562 individuals, pooled urine samples or even wastewater samples for assessing the use of these  
563 designer drugs in the emerging research field of wastewater-based drug epidemiology [46].  
564 Since the data indicated that the *in vitro* metabolism of the targeted designer drugs proceeds  
565 at slow rate, the parent drug itself appears to be the key biomarker in most cases. However,  
566 for PMA and PMMA, the respective *para*-hydroxylated metabolite can be considered as its  
567 second target biomarker. Also, it should be noted that since PMMA-M2 (i.e. PMA) was only



568 the secondary metabolite of PMMA, high levels of PMA detection in human fluids and  
569 wastewater samples may reflect the use PMA rather than that of PMMA. From the current *in*  
570 *vitro* experiments of 4-MTA, 4-methylthiocathine (4-MTA-M1) can be regarded as its key  
571 biomarker, with the di-hydroxylated metabolite (4-MTA-M4) as its second major biomarker.  
572 In future studies, *in vitro* experiments can provide further support to identify suitable  
573 biomarkers in the matrix of interest. For this purpose, the database of retention times, MS and  
574 MS/MS spectra of each metabolite detected *in vitro* represents a valuable tool to confirm the  
575 identity of the biomarkers detected in (*in vivo*) samples, particularly when no authentic  
576 reference standards for any of these metabolites/biomarkers are commercially available. It  
577 should be noted that further research is needed to examine whether those potential  
578 biomarkers are stable in wastewater before they can be used for reliable monitoring of drug  
579 use in wastewater-based drug epidemiology.

580

## 581 **5. Conclusions**

582 Overall, the work of this study has, for the first time, (a) screened for human *in vitro*  
583 metabolites of the selected phenethylamine-based designer drugs using an untargeted analysis  
584 of LC-QTOF-MS, and also (b) described a stepwise *in vitro* experimental design to enhance  
585 the reliability of assessing *in vitro* drug metabolism. The metabolism of the targeted drugs  
586 was mainly catalysed by CYP enzymes and progressed at relatively slow rate with only  
587 limited number of metabolites formed. The *in vitro* metabolism pathway of the selected drugs  
588 preferentially proceeded via *O*-dealkylation followed by *N*-dealkylation, and to a much  
589 smaller extent, oxidation of unsubstituted carbon atoms and oxidative deamination. The *in*  
590 *vitro* metabolism results broadly agreed with the findings of other available metabolism  
591 studies for phenethylamine-based drugs. The current work has established a list of specific *in*  
592 *vitro* human metabolites for the targeted drugs which are beneficial to all kinds of drug-  
593 related disciplines, such as clinical and forensic toxicology and the emerging research field of

594 wastewater-based drug epidemiology, for better detection and monitoring of the use of these  
595 drugs in humans and communities.

596

### 597 **Acknowledgements**

598 The National Research Centre for Environmental Toxicology (Entox) is a joint venture  
599 of The University of Queensland (UQ) and Queensland Health Forensic Scientific Services  
600 (QHFSS). The authors sincerely thank Nele Van den Eede (University of Antwerp (UA)) and  
601 Walid Maho (UA) for advising on the operation of the LC-QTOF-MS instrument. We also  
602 would like to acknowledge Xiaobo Zheng (UA) for assistance with the sample preparation  
603 and Maria Jose Gomez Ramos (Entox, UQ) and Nele Van den Eede for the discussion on  
604 fragmentation in mass spectrometry. We sincerely thank Dr. Raimondo Bruno (University of  
605 Tasmania, Australia) for his valuable input on discussions and language revisions. Foon Yin  
606 Lai is funded through UQ Collaboration and Industry Engagement Fund (UQCIEF #608290)  
607 and Collaborative Research Seeding Grants of the Faculty of Health and Behavioural  
608 Sciences (UQHABS #608670). Alexander L.N. van Nuijs acknowledges FWO Flanders for  
609 his scholarship. The research leading to these results has received funding from the European  
610 Union Seventh Framework Programme (FP7/2007-2013) under grant agreement #295138  
611 (INTERFLAME project), #316665 (A-TEAM project) and #317205 (SEWPROF project).

612

### 613 **Conflict of interest**

614 None

615 **References**

- 616 [1] UNODC. World Drug Report 2013. United Nations Office of Drugs and Crime (UNODC), United Nations  
617 publication, Sales No E13XI6, 2013.
- 618 [2] UNODC. The Challenge of New Psychoactive Substances. United Nations Office of Drugs and Crime  
619 (UNODC), A Report from the Global SMART Programme, March 2013.
- 620 [3] L.A. King, A.T. Kicman. A brief history of 'new psychoactive substances'. *Drug Test Anal* 3 (2011) 401-3.
- 621 [4] I. Sample. 'Superman' pill deaths spark calls for dangerous-drugs alert system. *The Guardian* 17 January  
622 2015. Available at: [http://www.theguardian.com/society/2015/jan/16/superman-pill-deaths-dangerous-drugs-](http://www.theguardian.com/society/2015/jan/16/superman-pill-deaths-dangerous-drugs-alert-system)  
623 [alert-system](http://www.theguardian.com/society/2015/jan/16/superman-pill-deaths-dangerous-drugs-alert-system) [accessed 26 February 2015]
- 624 [5] D. Nutt. The Superman pill deaths are the result of our illogical drugs policy *The Guardian* 5 January 2015.  
625 Available at: [http://www.theguardian.com/commentisfree/2015/jan/05/superman-pill-ecstasy-pma-deaths-drugs-](http://www.theguardian.com/commentisfree/2015/jan/05/superman-pill-ecstasy-pma-deaths-drugs-policy)  
626 [policy](http://www.theguardian.com/commentisfree/2015/jan/05/superman-pill-ecstasy-pma-deaths-drugs-policy) [accessed 26 February 2015]
- 627 [6] Australian Broadcasting Corporation (ABC). Potentially lethal 'Superman' drug could be on sale in Australia,  
628 police warn. ABC 25 February 2015 Available at:  
629 <http://www.theguardian.com/commentisfree/2015/jan/05/superman-pill-ecstasy-pma-deaths-drugs-policy>  
630 [accessed 26 February 2015]
- 631 [7] E. Zuccato, C. Chiabrando, S. Castiglioni, *et al.* Estimating community drug abuse by wastewater analysis.  
632 *Environ Health Perspect* 116 (2008) 1027-32.
- 633 [8] K.V. Thomas, L. Bijlsma, S. Castiglioni, *et al.* Comparing illicit drug use in 19 European cities through  
634 sewage analysis. *Sci Total Environ* 432 (2012) 432-9.
- 635 [9] C. Chen, C. Kostakis, R.J. Irvine, *et al.* Increases in use of novel synthetic stimulant are not directly linked to  
636 decreased use of 3,4-methylenedioxy-*N*-methylamphetamine (MDMA). *Forensic Sci Int* 231 (2013) 278-83.
- 637 [10] A.L.N. van Nuijs, A. Gheorghe, P.G. Jorens, *et al.* Optimization, validation, and the application of liquid  
638 chromatography-tandem mass spectrometry for the analysis of new drugs of abuse in wastewater. *Drug Test*  
639 *Anal* 6 (2014) 861-7.
- 640 [11] M.J. Reid, L. Derry, K.V. Thomas. Analysis of new classes of recreational drugs in sewage: Synthetic  
641 cannabinoids and amphetamine-like substances. *Drug Test Anal* 6 (2014) 72-9.
- 642 [12] A. Kankaanpää, K. Ariniemi, M. Heinonen, *et al.* Use of illicit stimulant drugs in Finland: a wastewater  
643 study in ten major cities. *Sci Total Environ* 487 (2014) 696-702.
- 644 [13] J. Kinyua, A. Covaci, W. Maho, *et al.* Sewage-based epidemiology in monitoring the use of new  
645 psychoactive substances: Validation and application of an analytical method using LC-MS/MS. *Drug Test Anal*  
646 (2015). DOI: 10.1002/dta.1777.
- 647 [14] Peters FT, Meyer MR. *In vitro* approaches to studying the metabolism of new psychoactive compounds.  
648 *Drug Test Anal* 3 (2011) 483-95.
- 649 [15] Z.Y. Liu. An introduction to hybrid ion trap/time-of-flight mass spectrometry coupled with liquid  
650 chromatography applied to drug metabolism studies. *J Mass Spectrom* 47 (2012) 1627-42.
- 651 [16] D. Spaggiari, L. Geiser, S. Rudaz. Coupling ultra-high-pressure liquid chromatography with mass  
652 spectrometry for in-vitro drug-metabolism studies. *Trac-Trend Anal Chem* 63 (2014) 129-39.
- 653 [17] European Monitoring Center for Drugs and Drug Addiction (EMCDDA). Action on new drugs. Risk  
654 assessments. EMCDDA, Lisbon. Available at: <http://www.emcdda.europa.eu/html.cfm/index16776EN.html>  
655 [accessed 26 February 2015].
- 656 [18] M.V. Bach, R.T. Coutts, G.B. Baker. Involvement of CYP2D6 in the *in vitro* metabolism of amphetamine,  
657 two *N*-alkylamphetamines and their 4-methoxylated derivatives. *Xenobiotica* 29 (1999) 719-32.
- 658 [19] R.F. Staack, D.S. Theobald, L.D. Paul, *et al.* Identification of human cytochrome P450 2D6 as major enzyme  
659 involved in the *O*-demethylation of the designer drug *p*-methoxymethamphetamine. *Drug Metab Dispos* 32  
660 (2004) 379-81.
- 661 [20] R.T. Coutts, O.O. Bolaji, P. Su, *et al.* Metabolism of methoxyphenamine *in vitro* by a CYP2D6 microsomal  
662 preparation. *Drug Metab Dispos* 22 (1994) 756-60.
- 663 [21] H.H. Maurer, J. Bickeboeller-Friedrich, T. Kraemer, *et al.* Toxicokinetics and analytical toxicology of  
664 amphetamine-derived designer drugs ('Ecstasy'). *Toxicol Lett* 112-113 (2000) 133-42.
- 665 [22] M.R. Meyer, F.T. Peters, H.H. Maurer. Stereoselective differences in the cytochrome P450-dependent  
666 dealkylation and demethylation of *N*-methyl-benzodioxolyl-butanamine (MBDB, Eden) enantiomers.  
667 *Biochem Pharmacol* 77 (2009) 1725-34.
- 668 [23] M.R. Meyer, F.T. Peters, H.H. Maurer. Investigations on the human hepatic cytochrome P450 isozymes  
669 involved in the metabolism of 3,4-methylenedioxy-amphetamine (MDA) and benzodioxolyl-butanamine (BDB)  
670 enantiomers. *Toxicol Lett* 190 (2009) 54-60.
- 671 [24] N. van den Eede, W. Maho, C. Erratico, *et al.* First insights in the metabolism of phosphate flame  
672 retardants and plasticizers using human liver fractions. *Toxicol Lett* 223 (2013) 9-15.
- 673 [25] A. Ballesteros-Gómez, C. Erratico, N. van den Eede, *et al.* *In vitro* metabolism of 2-ethylhexyldiphenyl  
674 phosphate (EHDPHP) by human liver microsomes. *Toxicol Lett* 232 (2015) 203-12.

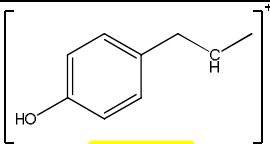
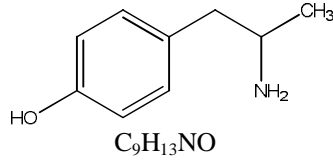
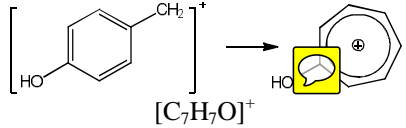

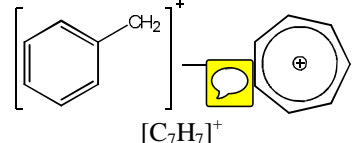
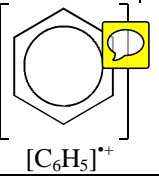
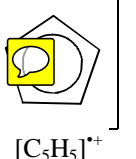
- 675 [26] E. Tyrkkö, A. Pelander, R. Ketola, *et al.* *In silico* and *in vitro* metabolism studies support identification of  
676 designer drugs in human urine by liquid chromatography/quadrupole-time-of-flight mass spectrometry. *Anal*  
677 *Bioanal Chem* 405 (2013) 6697-709.
- 678 [27] B. Chiavarino, M.E. Crestoni, O. Dopfer, *et al.* Benzylum versus tropylium ion dichotomy: vibrational  
679 spectroscopy of gaseous  $C_8H_9^+$  ions. *Angew Chem Int Edit* 51 (2012) 4947-9.
- 680 [28] P.R. Schreiner, H.P. Reisenauer, J. Romanski, *et al.* A formal carbon-sulfur triple bond:  $H-C\equiv S-O-H$ .  
681 *Angew Chem Int Edit* 48 (2009) 8133-6.
- 682 [29] N. Chauret, A. Gauthier, D.A. Nicoll-Griffith. Effect of common organic solvents on *in vitro* cytochrome  
683 P450-mediated metabolic activities in human liver microsomes. *Drug Metab Dispos* 26 (1998) 1-4.
- 684 [30] D. Li, Y. Han, X. Meng, *et al.* Effect of regular organic solvents on cytochrome P450-mediated metabolic  
685 activities in rat liver microsomes. *Drug Metab Dispos* 38 (2010) 1922-5.
- 686 [31] J.T. Wu, L.H. Wu, J.A. Knight. Stability of NADPH: effect of various factors on the kinetics of  
687 degradation. *Clin Chem* 32 (1986) 314-9.
- 688 [32] R.S. Obach. Nonspecific binding to microsomes: impact on scale-up of *in vitro* intrinsic clearance to  
689 hepatic clearance as assessed through examination of warfarin, imipramine, and propranolol. *Drug Metab*  
690 *Dispos* 25 (1997) 1359-69.
- 691 [33] K. Venkatakrisnan, L.L. von Moltke, R.S. Obach, *et al.* Microsomal binding of amitriptyline: effect on  
692 estimation of enzyme kinetic parameters *in vitro*. *J Pharmacol Exp Ther* 293 (2000) 343-50.
- 693 [34] R. Baselt. *Disposition of Toxic Drugs and Chemicals in Man*. Foster City, CA: Biomedical Publications;  
694 (2008).
- 695 [35] L.G. Dring, R.L. Smith, R.T. Williams. The metabolic fate of amphetamine in man and other species.  
696 *Biochem J* 116 (1970) 425-35.
- 697 [36] I. Kim, J.M. Oyler, E.T. Moolchan, *et al.* Urinary pharmacokinetics of methamphetamine and its  
698 metabolite, amphetamine following controlled oral administration to humans. *Ther Drug Monit* 26 (2004) 664-  
699 72.
- 700 [37] I. Kitchen, J. Tremblay, J. André, *et al.* Interindividual and interspecies variation in the metabolism of the  
701 hallucinogen 4-methoxyamphetamine. *Xenobiotica* 9 (1979) 397-404.
- 702 [38] R.F. Staack, H.H. Maurer. Metabolism of designer drugs of abuse. *Curr Drug Metab* 6 (2005) 259-74.
- 703 [39] R.F. Staack, J. Fehn, H.H. Maurer. New designer drug *p*-methoxymethamphetamine: studies on its  
704 metabolism and toxicological detection in urine using gas chromatography-mass spectrometry. *J Chromatogr B*  
705 789 (2003) 27-41.
- 706 [40] H. Carmo, J. Hengstler, D. de Boer, *et al.* Comparative metabolism of the designer drug 4-  
707 methylthioamphetamine by hepatocytes from man, monkey, dog, rabbit, rat and mouse. *N-S Arch Pharmacol*  
708 369 (2004) 198-205.
- 709 [41] A.H. Ewald, F.T. Peters, M. Weise, *et al.* Studies on the metabolism and toxicological detection of the  
710 designer drug 4-methylthioamphetamine (4-MTA) in human urine using gas chromatography-mass  
711 spectrometry. *J Chromatogr B* 824 (2005) 123-31.
- 712 [42] H. Carmo, D. de Boer, F. Remião, *et al.* Identification of 4-methylthioamphetamine and some of its  
713 metabolites in mouse urine by GC-MS after acute administration. *J Anal Toxicol* 26 (2002) 228-32.
- 714 [43] H.H. Maurer. On the metabolism and the toxicological analysis of methylenedioxyphenylalkylamine  
715 designer drugs by gas chromatography-mass spectrometry. *Ther Drug Monit* 18 (1996) 465-70.
- 716 [44] Kronstrand R. *Emerging Designer Drug Monograph*. Society of Forensic Toxicologists, Inc Designer Drug  
717 Committee Monographs vers 11, 2013.
- 718 [45] Welter J., Kavanagh P., Meyer M., *et al.* Benzofuran analogues of amphetamine and methamphetamine:  
719 studies on the metabolism and toxicological analysis of 5-APB and 5-MAPB in urine and plasma using GC-MS  
720 and LC-(HR)-MS<sup>n</sup> techniques. *Anal Bioanal Chem* (2014) 1-18.
- 721 [46] A.L.N. van Nuijs, S. Castiglioni, I. Tarcomnicu, *et al.* Illicit drug consumption estimations derived from  
722 wastewater analysis: A critical review. *Sci Total Environ* 409 (2011) 3564-77.

723

724  
725  
726

## Tables

**Table 1:** Postulated structure for PMA metabolite generated from incubation with HLM in tier I.

ID Met	Precursor ion (MS-TOF)			RT (min)	Product ions* (MS/MS-TOF)			Proposed structure
	Measured m/z [M+H] <sup>+</sup>	Expected m/z (ppm diff.)	Measured DBE		Measured m/z	Expected m/z (ppm diff.)	Potential fragment structure [molecular formula]	
M1	152.1063 [C <sub>9</sub> H <sub>13</sub> NO + H] <sup>+</sup>	152.1070 (+4.60)	4	5.17	135.0799	135.0810 (-8.14)	 [C <sub>9</sub> H <sub>11</sub> O] <sup>+</sup>	 C <sub>9</sub> H <sub>13</sub> NO
					107.0495	107.0497 (-1.87)	 [C <sub>7</sub> H <sub>7</sub> O] <sup>+</sup>	
					91.0552	91.0548 (+4.39)	 [C <sub>7</sub> H <sub>7</sub> ] <sup>+</sup>	
					77.0390	77.0386 (+5.19)	 [C <sub>6</sub> H <sub>5</sub> ] <sup>+</sup>	
					65.0364	65.0386 (-33.8)	 [C <sub>5</sub> H <sub>5</sub> ] <sup>+</sup>	

ID Met: Identified metabolite; m/z: mass to charge ratio; DBE: double bond equivalents.

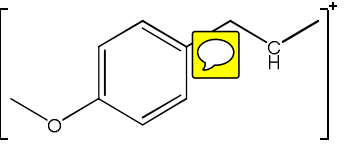

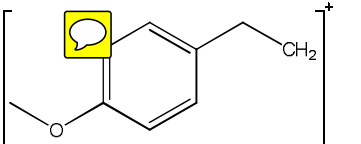
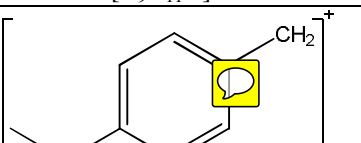
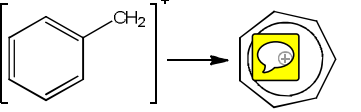
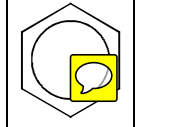
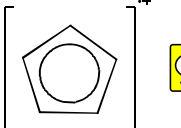
\*See Fig. S1 for the MS/MS-TOF spectrum.

727

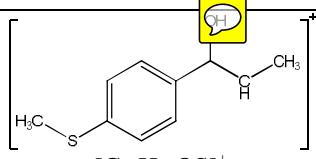
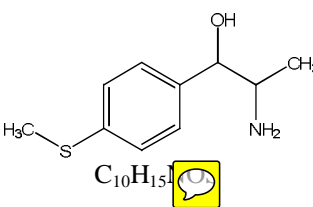
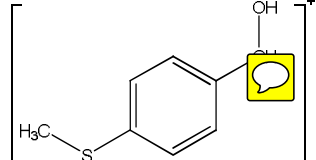
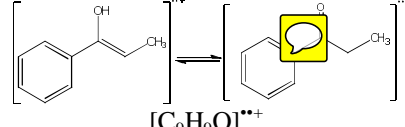
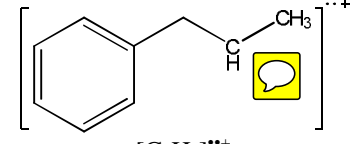
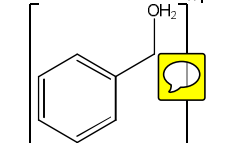
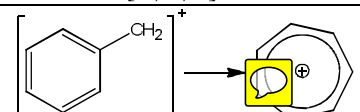
728

**Table 2:** Postulated structures for PMMA metabolites generated from incubation with HLM in tier I.

ID Met	Precursor ion (MS-TOF)				Product ions* (MS/MS-TOF)			Proposed structure
	Measured m/z [M+H] <sup>+</sup>	Expected m/z (ppm diff.)	Measured DBE	RT (min)	Measured m/z	Expected m/z (ppm diff.)	Potential fragment structure [molecular formula]	
M1	166.1234 [C <sub>10</sub> H <sub>15</sub> NO +H] <sup>+</sup>	166.1226 (+4.82)	4	5.40	135.0798	135.0810 (-8.88)	 [C <sub>9</sub> H <sub>11</sub> O] <sup>+</sup>	 C <sub>10</sub> H <sub>15</sub> NO
					119.0472	119.0497 (-21.0)	 [C <sub>8</sub> H <sub>7</sub> O] <sup>+</sup>	
					107.0483	107.0497 (-13.1)	 [C <sub>7</sub> H <sub>7</sub> O] <sup>+</sup>	
					91.0540	91.0548 (-8.79)	 [C <sub>7</sub> H <sub>7</sub> ] <sup>+</sup>	
					77.0383	77.0386 (+3.89)	 [C <sub>6</sub> H <sub>5</sub> ] <sup>+</sup>	
					65.0380	65.0386 (-9.23)	 [C <sub>5</sub> H <sub>5</sub> ] <sup>+</sup>	

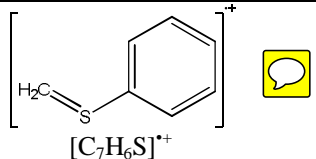
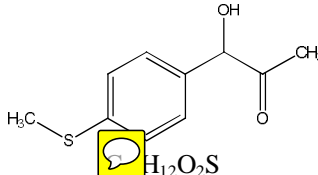
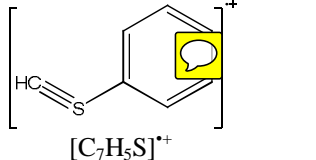
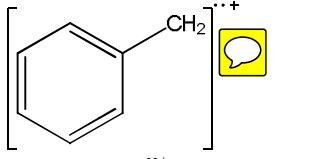
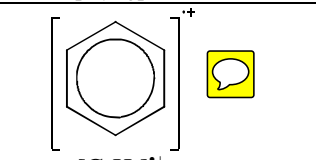
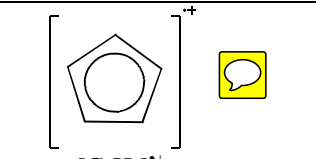
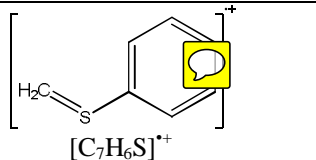
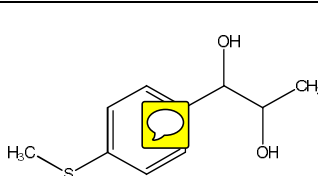
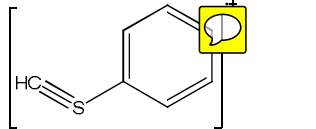
M2	166.1208 [C <sub>10</sub> H <sub>15</sub> NO + H] <sup>+</sup>	166.1226 (+10.8)	4	15.6	149.0931	149.0966 (-23.5)	 [C <sub>10</sub> H <sub>13</sub> O] <sup>+</sup>	 C <sub>10</sub> H <sub>15</sub> NO
					135.0790	135.0810 (-14.8)	 [C <sub>9</sub> H <sub>11</sub> O] <sup>+</sup>	
					121.0625	121.0653 (-23.1)	 [C <sub>8</sub> H <sub>9</sub> O] <sup>+</sup>	
					91.0523	91.0548 (-27.5)	 [C <sub>7</sub> H <sub>7</sub> ] <sup>+</sup>	
					77.0371	77.0386 (-19.5)	 [C <sub>6</sub> H <sub>5</sub> ] <sup>+</sup>	
					65.0364	65.0386 (-33.8)	 [C <sub>5</sub> H <sub>5</sub> ] <sup>+</sup>	
<p>ID Met: Identified metabolite; m/z: mass to charge ratio; DBE: double bond equivalents.  *See Figs. S2A and S2B for the MS/MS-TOF spectrum.</p>								

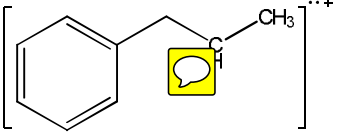
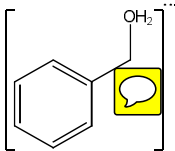
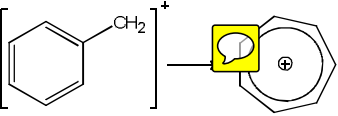
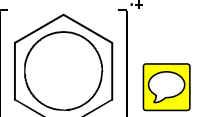
730 **Table 3:** Postulated structures for 4-MTA metabolites generated from incubation with HLM in tier I.

ID Met	Precursor ion (MS-TOF)				Product ions* (MS/MS-TOF)			Proposed structure
	Measured m/z [M+H] <sup>+</sup>	Expected m/z (ppm diff.)	Measured DBE	RT (min)	Measured m/z	Expected m/z (ppm diff.)	Potential fragment structure [molecular formula]	
M1	198.0946 [C <sub>10</sub> H <sub>15</sub> NOS +H] <sup>+</sup>	198.0947 (-0.50)	4	6.20	181.0674	181.0687 (-7.18)	 [C <sub>10</sub> H <sub>13</sub> OS] <sup>+</sup>	 C <sub>10</sub> H <sub>15</sub> NOS
					153.0362	153.0374 (-7.84)	 [C <sub>8</sub> H <sub>9</sub> OS] <sup>+</sup>	
					133.0639	133.0648 (-6.76)	 [C <sub>9</sub> H <sub>9</sub> O] <sup>***+</sup>	
					117.0690	117.0699 (-7.69)	 [C <sub>9</sub> H <sub>9</sub> ] <sup>***+</sup>	
					107.0490	107.0491 (-0.93)	 [C <sub>7</sub> H <sub>7</sub> O] <sup>***+</sup>	
					91.0544	91.0548 (-4.39)		

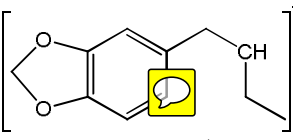
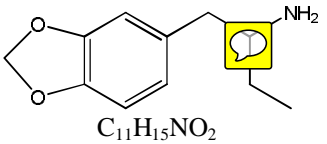
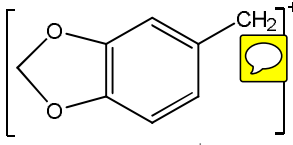
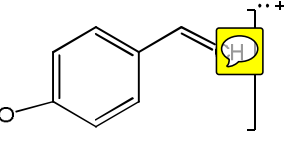
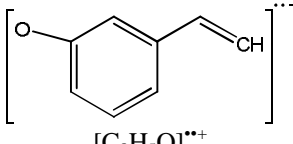
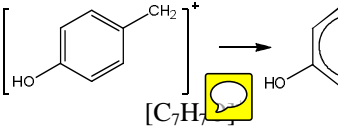
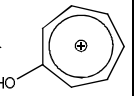
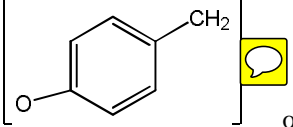


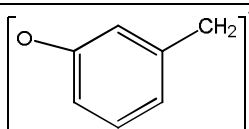
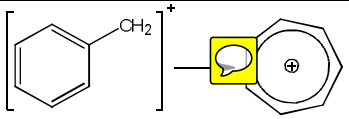
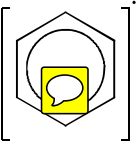
							$[C_7H_7]^+$	
					77.0382	77.0386 (-5.19)		
					65.0391	65.0386 (+7.69)		
M2	168.0836 $[C_9H_{13}NS + H]^+$	168.0841 (-2.97)	4	8.94	151.0558	151.0581 (-15.2)		
					117.0692	117.0699 (-5.98)		
					91.0536	91.0548 (-13.2)		
M3	197.0633 $[C_{10}H_{12}O_2S + H]^+$	197.0631 (+1.01)	5	14.1	137.0411	137.0425 (-10.2)		

					122.0184	122.0185 (-0.82)	 $[C_7H_6S]^+$	 $H_{12}O_2S$
					121.0095	121.0106 (-9.09)	 $[C_7H_5S]^+$	
					89.0389	89.0386 (+3.37)	 $[C_7H_5]^{3+}$	
					77.0385	77.0386 (-1.30)	 $[C_6H_5]^+$	
					65.0388	65.0386 (+3.08)	 $[C_5H_5]^+$	
M4	199.0787 $[C_{10}H_{14}O_2S + H]^+$	199.0787 (0.00)	4	15.4	122.0156	122.0185 (-23.8)	 $[C_7H_6S]^+$	 $C_{10}H_{14}O_2S$
					121.0097	121.0106 (-7.44)		

							$[C_7H_5S]^+$	731
					117.0712	117.0699 (+11.1)	 $[C_9H_9]^{2+}$	732
					107.0491	107.0491 (0.00)	 $[C_7H_7O]^{2+}$	
					91.0547	91.0548 (-1.10)	 $[C_7H_7]^+$	
					77.0375	77.0386 (-14.3)	 $[C_6H_5]^+$	
ID Met: Identified metabolite; m/z: mass to charge ratio; DBE: double bond equivalents. *See Figs. S3A to 3D for the MS/MS-TOF spectrum.								

733 **Table 4:** Postulated structure for MBDB metabolite generated from incubation with HLM in tier I.

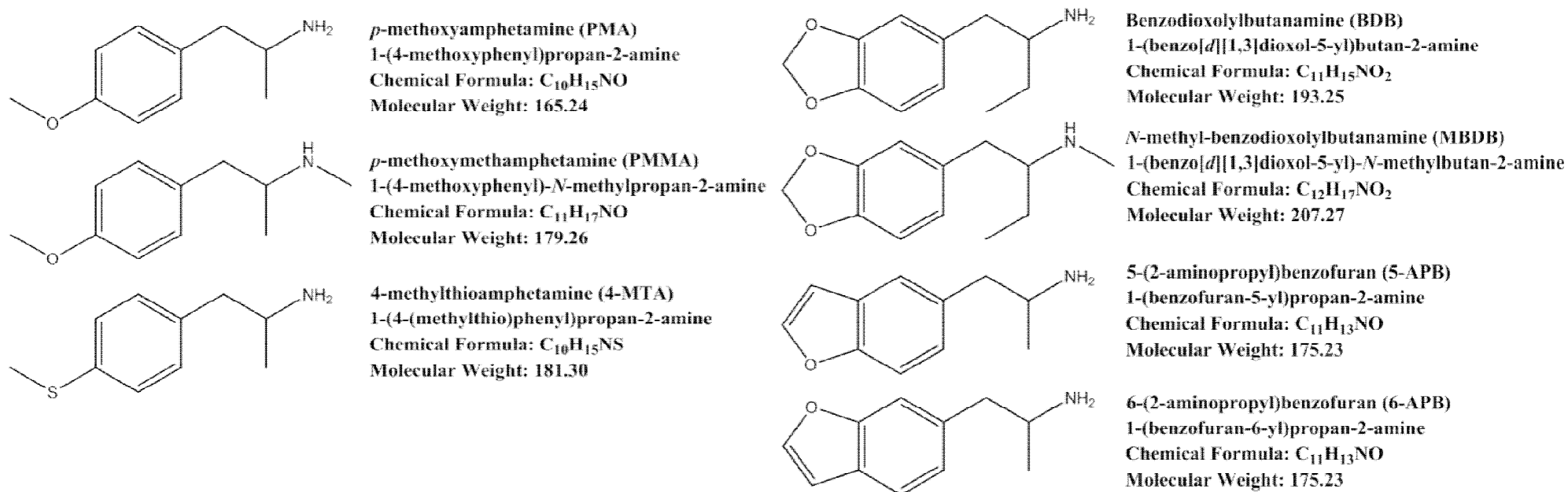
ID Met	Precursor ion (MS-TOF)				Product ions* (MS/MS-TOF)			Proposed structure
	Measured m/z [M+H] <sup>+</sup>	Expected m/z (ppm diff.)	Measured DBE	RT (min)	Measured m/z	Expected m/z (ppm diff.)	Potential fragment structure [molecular formula]	
M1	194.1174 [C <sub>11</sub> H <sub>15</sub> NO <sub>2</sub> +H] <sup>+</sup>	194.1176 (+1.03)	5	18.7	177.0894	177.0916 (-12.4)	 [C <sub>11</sub> H <sub>13</sub> O <sub>2</sub> ] <sup>+</sup>	 C <sub>11</sub> H <sub>15</sub> NO <sub>2</sub>
					135.0447	135.0446 (+0.74)	 [C <sub>8</sub> H <sub>7</sub> O <sub>2</sub> ] <sup>+</sup>	
					117.0327	117.0335 (-6.84)	 or  [C <sub>8</sub> H <sub>5</sub> O] <sup>++</sup>	
					107.0499	107.0497 (+1.87)	 [C <sub>7</sub> H <sub>7</sub> ] <sup>+</sup> → 	
					105.0329	105.0335 (-5.71)	 or	

							 $[C_7H_5O]^{**+}$
					91.0526	91.0548 (-24.2)	 $[C_7H_7]^+$
					77.0391	77.0386 (+6.49)	 $[C_6H_5]^+$
ID Met: Identified metabolite; m/z: mass to charge ratio; DBE: double bond equivalents. *See Fig. S4 for the MS/MS-TOF spectrum.							

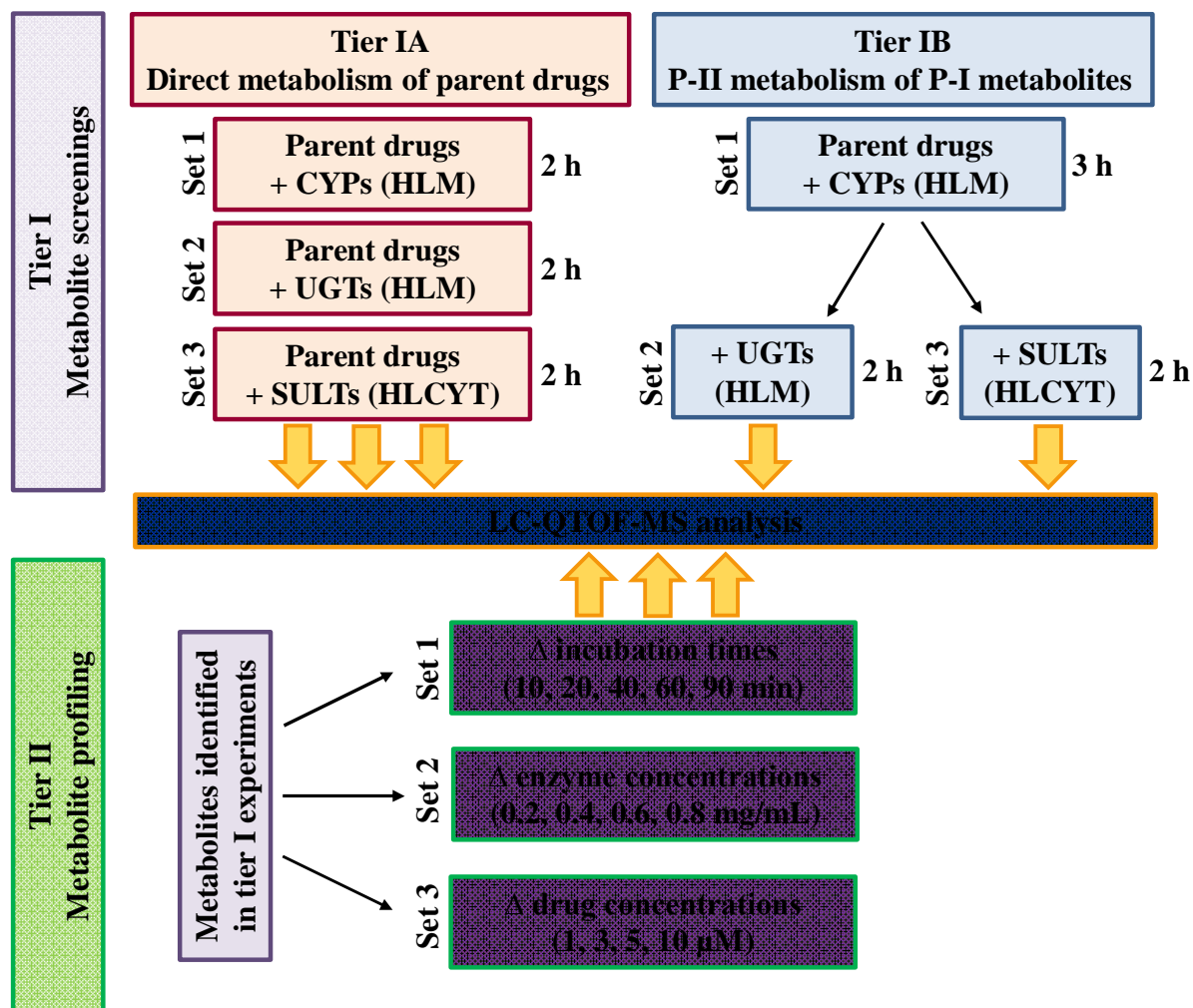
734  
735

736  
737

## Figures

738  
739  
740**Figure 1:** Seven phenethylamine-based designer drugs selected for this study.

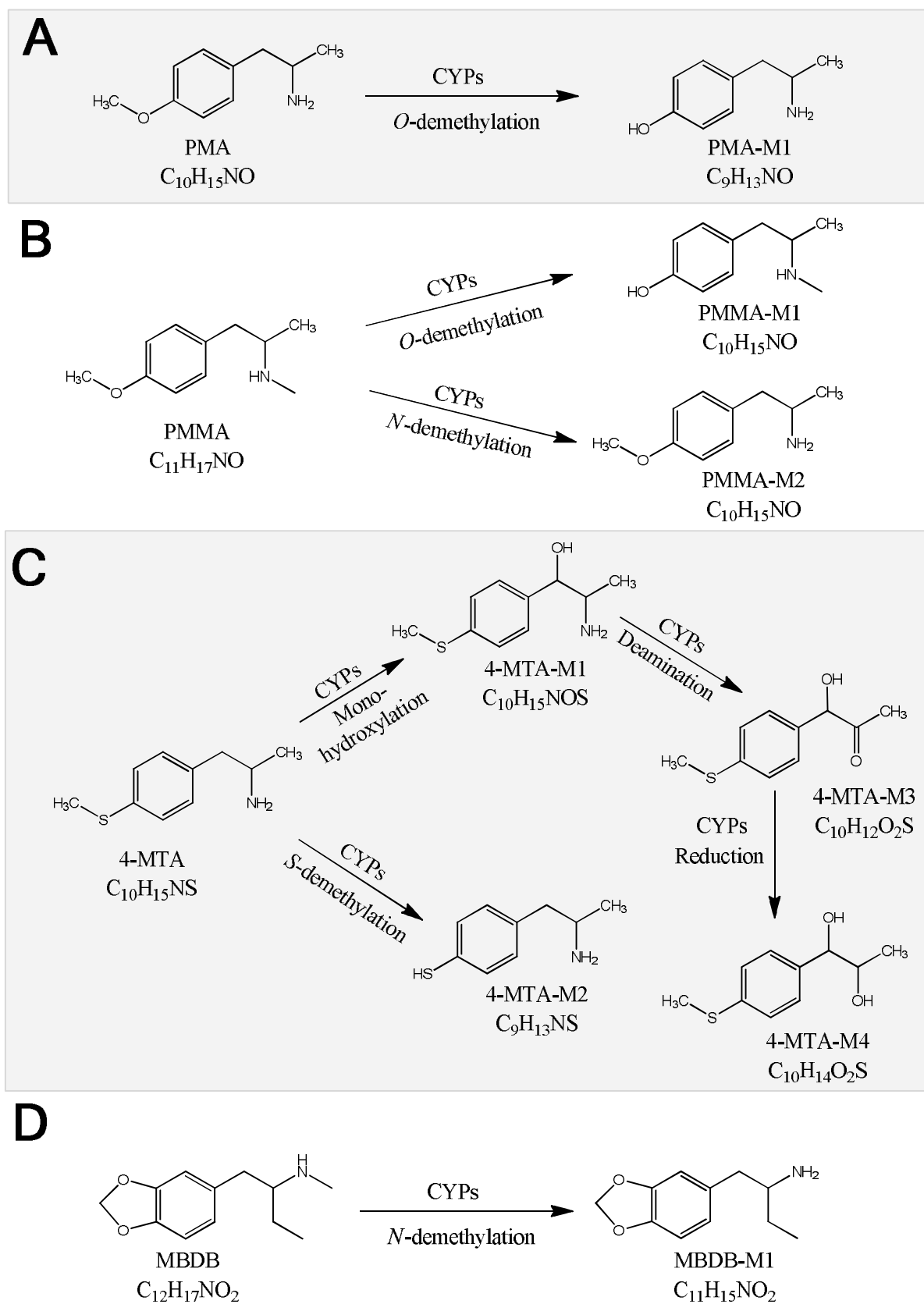
741



742  
 743  
 744  
 745  
 746  
 747

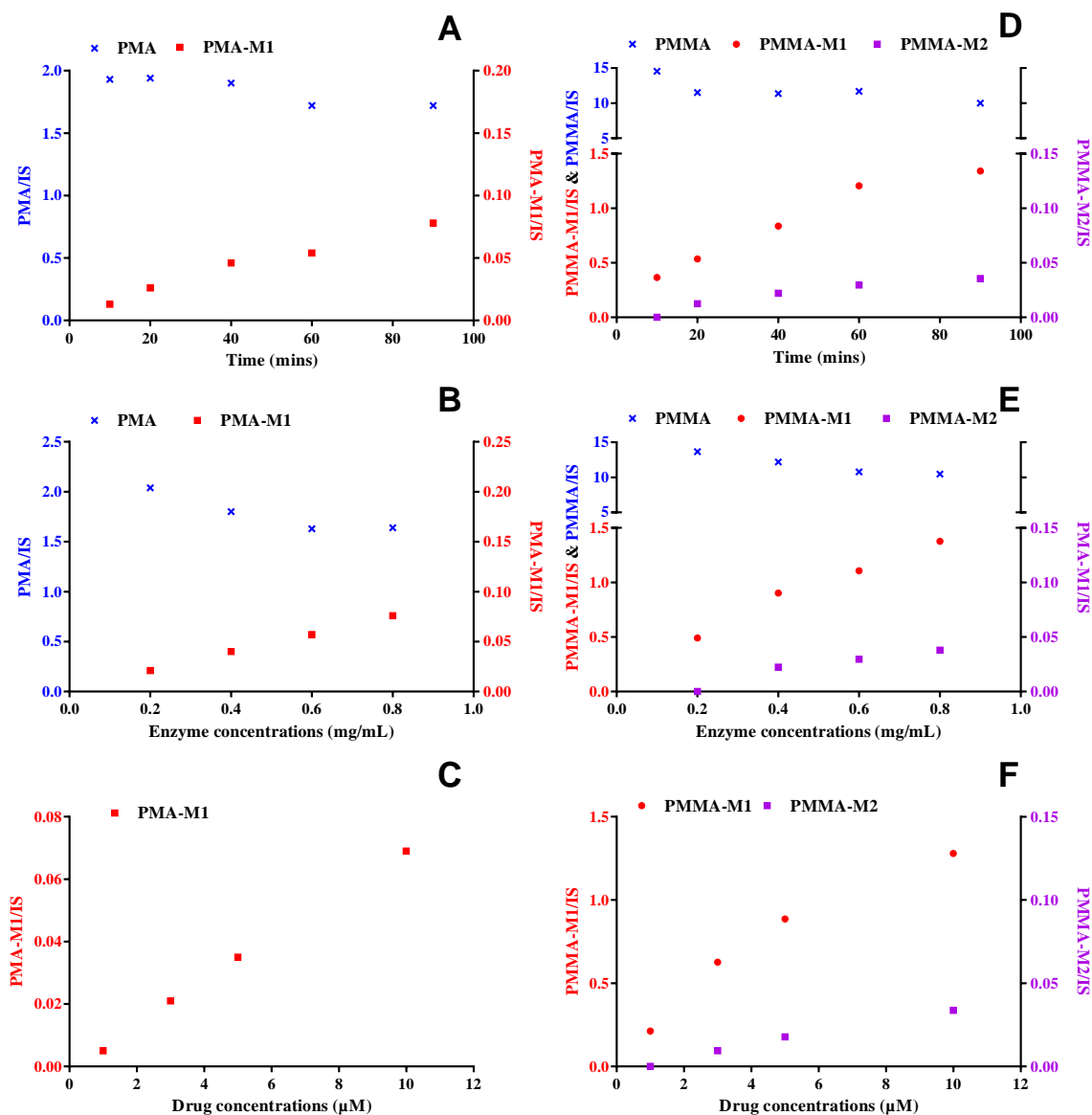
**Figure 2:** Schematic flow of the two-tiered approach on human *in vitro* drug metabolism in this study. P-I: Phase I; P-II: Phase II; HLM: human liver microsomes; HLCYT: human liver cytosol. The corresponding family of enzymes (i.e. CYPs, UGTs and SULTs) is described in section 2.2.

748

749  
750  
751  
752  
753

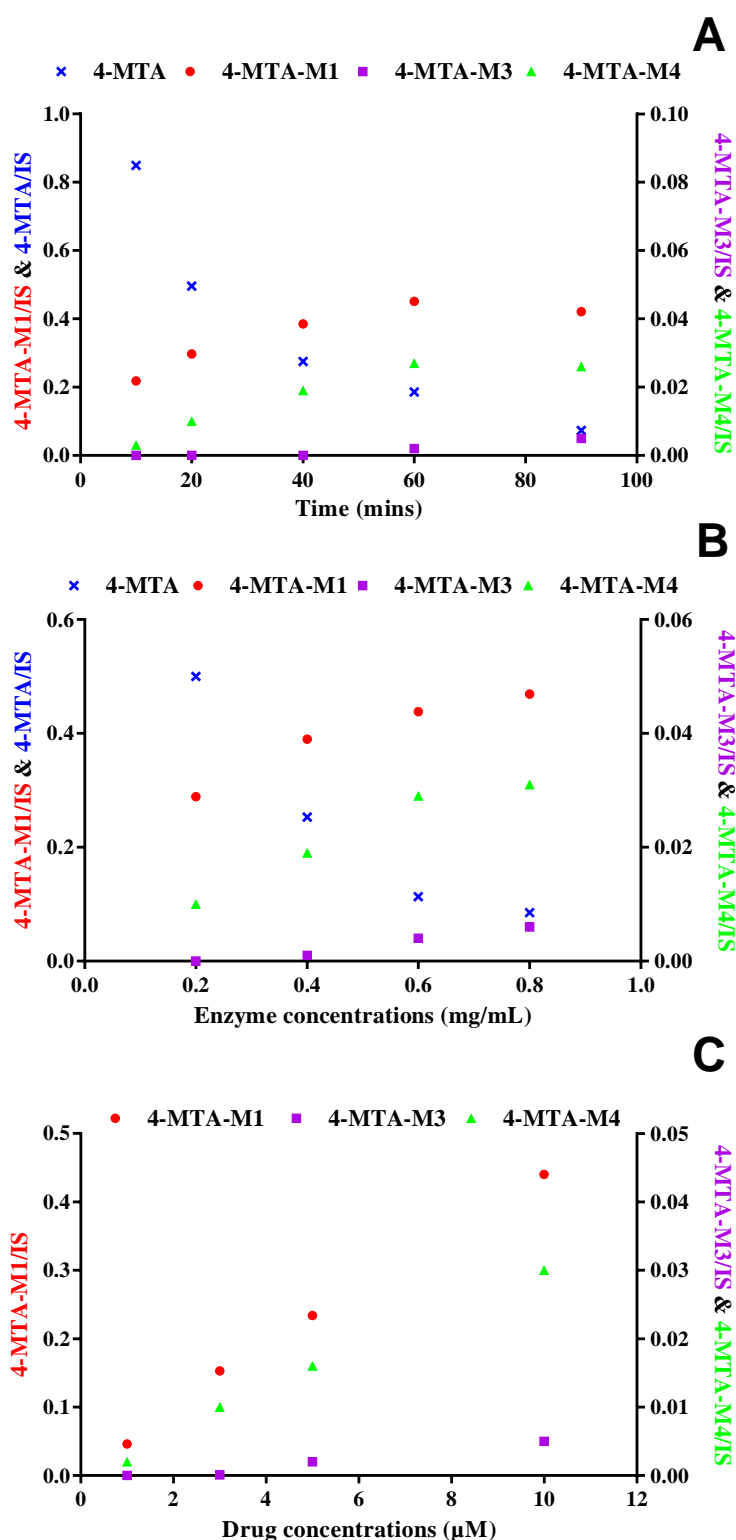
**Figure 3:** Proposed biotransformation pathways of PMA (A), PMMA (B), 4-MTA (C) and MBDB (D) by human CYP enzymes.



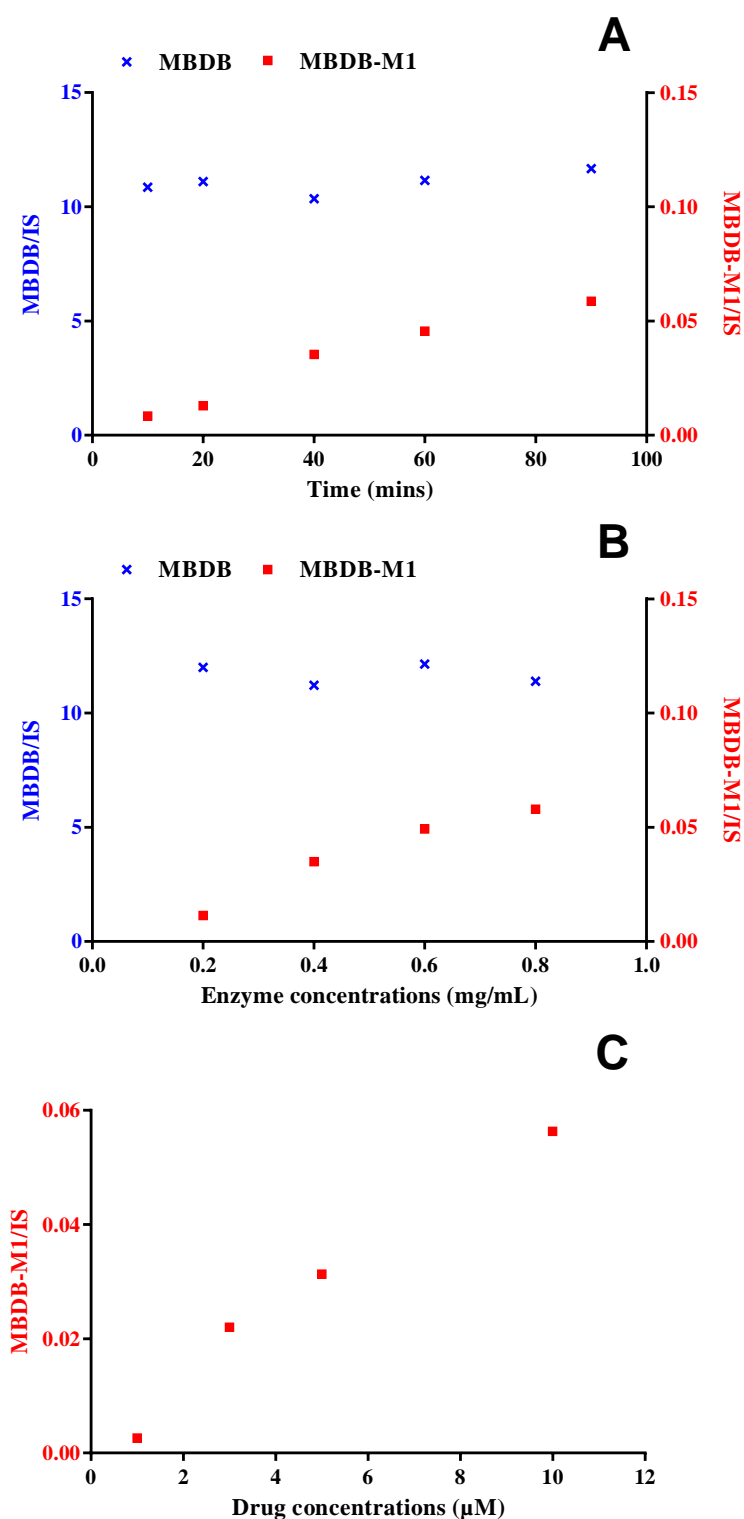


754  
 755 **Figure 4:** Metabolic profiles of PMA and its metabolite (A–C) and PMMA and its metabolites (D–F) under  
 756 three different testing conditions (i.e. changes in the experimental times, enzyme concentrations and drug  
 757 concentrations) in the tier II experiment. The response presents as the peak area ratio of the metabolites or  
 758 parent drug to the internal standards. Note: when testing with the change in experimental times (i.e. A and D),  
 759 the enzyme and substrate concentration was kept at 0.8 mg/mL and 10 µM, respectively; when testing with the  
 760 change in the enzyme concentrations (i.e. B and E), the substrate concentration was kept at 10 µM and the  
 761 experimental time was conducted for 90 min; when testing with the change in the substrate concentrations (i.e.  
 762 C and F), the enzyme concentration was kept at 0.8 mg/mL and the experimental time was conducted for 90  
 763 min. See Tables 1 and 2 for the molecular structures of the metabolites.

764  
 765  
 766  
 767



768  
 769 **Figure 5:** Metabolic profiles of 4-MTA and its metabolites under three different testing conditions (i.e. changes  
 770 in the experimental times, enzyme concentrations and drug concentrations) in the tier II experiment. The  
 771 response presents as the peak area ratio of the metabolites or parent drug to the internal standards. Note: when  
 772 testing with the change in experimental times (i.e. A), the enzyme and substrate concentration was kept at 0.8  
 773 mg/mL and 10  $\mu$ M, respectively; when testing with the change in the enzyme concentrations (i.e. B), the  
 774 substrate concentration was kept at 10  $\mu$ M and the experimental time was conducted for 90 min; when testing  
 775 with the change in the substrate concentrations (i.e. C), the enzyme concentration was kept at 0.8 mg/mL and  
 776 the experimental time was conducted for 90 min. See Table 3 for the molecular structures of the metabolites.  
 777



778

779 **Figure 6:** Metabolic profiles of MBDB and its metabolite under three different testing conditions (i.e. changes  
 780 in the experimental times, enzyme concentrations and drug concentrations) in the tier II experiment. The  
 781 response presents as the peak area ratio of the metabolites or parent drug to the internal standards. Note: when  
 782 testing with the change in experimental times (i.e. A), the enzyme and substrate concentration was kept at 0.8  
 783 mg/mL and 10 µM, respectively; when testing with the change in the enzyme concentrations (i.e. B), the  
 784 substrate concentration was kept at 10 µM and the experimental time was conducted for 90 min; when testing  
 785 with the change in the substrate concentrations (i.e. C), the enzyme concentration was kept at 0.8 mg/mL and  
 786 the experimental time was conducted for 90 min. See Table 4 for the molecular structure of the metabolite.  
 787

778